MSL3 promotes germline stem cell differentiation in female *Drosophila*

Alicia McCarthy[1], Kahini Sarkar[1], Elliot T Martin[1], Maitreyi Upadhyay[1,2#], Seoyeon Jang[3], Nathan D Williams[3,4#], Paolo E Forni[1], Michael Buszczak[3], Prashanth Rangan[1*]

[1]Department of Biological Sciences/RNA Institute, University at Albany SUNY, Albany, NY 12202

[2#]Current address: Department of Stem Cell and Regenerative Biology, Harvard University, Cambridge, MA 02138

[3]Department of Molecular Biology, University of Texas Southwestern Medical Center, Dallas, TX 75390

[4#]Current address: Department of Cell Biology, Yale University School of Medicine, New Haven, CT 06520

*Corresponding Author and Lead Contact

Summary statement: A component of dosage compensation complex promotes germ line differentiation by regulating levels of a ribosomal protein in female *Drosophila*

Keywords: Differentiation, meiosis, MSL3, RpS19, SET2 and Rbfox1

Prashanth Rangan

Department of Biological Sciences/RNA Institute

University at Albany, SUNY

1400 Washington Avenue

Albany, NY 12222

Tel: 518 442 3485

Email: prangan@albany.edu

Abstract
Gamete formation from germline stem cells (GSCs) is essential for sexual reproduction. However, the regulation of GSC differentiation are incompletely understood. Set2, which deposits H3K36me3 modifications, is required for GSC differentiation during *Drosophila* oogenesis. We discovered that the H3K36me3 reader Male-specific lethal 3 (MSL3) and histone acetyltransferase complex Ada2a-containing (ATAC) cooperate with Set2 to regulate GSC differentiation in female *Drosophila*. MSL3, acting independent from the rest of the male specific lethal complex, promotes transcription of genes including a germline enriched *ribosomal protein S19* paralog, *RpS19b*. *RpS19b* upregulation is required for translation of RNA-binding Fox protein 1 (Rbfox1), a known meiotic cell cycle entry factor. Thus, MSL3 regulates GSC differentiation by modulating translation of a key factor that promotes transition to an oocyte fate.

Introduction
Germ cells give rise to gametes, a fundamental requirement for sexual reproduction. The production of gametes is tightly controlled to ensure a constant supply throughout the reproductive life of an organism (Cinalli et al., 2008; Kimble, 2011; Lehmann, 2012; Spradling et al., 1997). Germline stem cells (GSCs) divide mitotically to both self-renew and generate differentiating daughters that can enter meiosis (Kimble, 2011; Lehmann, 2012; Spradling et al., 2011). Loss of differentiation and meiotic entry results in infertility (Hughes et al., 2018; Lesch and Page, 2012; Soh et al., 2015).

GSC differentiation is well characterized during *Drosophila* oogenesis (Elizabeth T. Ables, 2015; Collins et al., 2014a). *Drosophila* ovaries are composed of individual egg producing units called ovarioles. A structure called the germarium lies at the tip of each ovariole and houses GSCs, which are marked by round organelles called spectrosomes (Eliazer and Buszczak, 2011; Morris and Spradling, 2011; Morrison and Spradling, 2008; Spradling et al., 2011, 2001, 2008) (**Fig. 1A**). GSCs both self-renew and differentiate into cystoblasts (CBs), which divide and undergo incomplete cytokinesis to give rise to 2-, 4-, 8-, and 16-cell cysts, which are marked by branched structures called fusomes (Chen and McKearin, 2003a, 2003b; Xie, 2013).

Early germ cell differentiation is controlled by both intrinsic and extrinsic factors (Flora et al., 2017; Spradling et al., 2011). The somatic niche of the germarium provides Decapentaplegic (DPP) signaling that leads to phosphorylation of Mothers against DPP (pMad) in GSCs, and transcriptional repression of the differentiation factor *bag of marbles* (*bam*) (Chen and McKearin, 2003a, 2003b; Kai and Spradling, 2003)). After GSC division, the CB is displaced from the niche, allowing for Bam expression (Chen

and McKearin, 2003a, 2003b). Bam is sufficient to promote the transition from CB to a differentiated 8-cell cyst (McKearin and Ohlstein, 1995; McKearin and Spradling, 1990).

In the 8-cell cyst, expression of cytoplasmic isoforms of RNA-binding Fox protein 1 (Rbfox1) leads to translational downregulation of self-renewal factors to promote expression of Bruno (Bru) (Carreira-Rosario et al., 2016; Tastan et al., 2010). Bru, in turn, translationally represses mitotic factors, which promote cyst divisions, and regulates entry into a meiotic cell cycle (Parisi et al., 2001; Sugimura and Lilly, 2006; Wang and Lin, 2007). Multiple cells in the cysts initiate meiosis, but only the oocyte will commit to meiosis; the other 15 cells acquire a nurse cell fate in the 16-cell cyst stage (Carpenter and Sandler, 1974; Huynh and St Johnston, 2004; Mach and Lehmann, 1997; Navarro et al., 2001; Theurkauf et al., 1993). The oocyte and the 15 nurse cells are encapsulated by somatic cells to form a developing egg chamber and eventually an egg (**Fig. 1A1**). Although Rbfox1 expression in the germline is essential for entry into a meiotic cell cycle and oocyte specification, how it is induced is unclear (Carreira-Rosario et al., 2016).

Another hallmark of meiosis, apart from a specialized cell cycle, is homologous chromosome recombination. This process is regulated by the formation of the synaptonemal complex (SC) (Elizabeth T Ables, 2015; Hughes et al., 2018). The SC starts to assemble on homologs in two cells with 4 ring canals, and to a lesser degree in the other 14 cells of the cyst and it then becomes restricted to the future oocyte (Page and Hawley, 2001; Von Stetina and Orr-Weaver, 2011) (**Fig. 1A**). While proper homologous recombination is not required for differentiation, it is required for fertility (Collins et al., 2014b; Handel and Schimenti, 2010). How transcription of SC components is activated during meiosis is not well understood.

GSC differentiation during *Drosophila* oogenesis requires the histone methyltransferase SET domain containing 2 (Set2), which confers histone H3 lysine 36 trimethylation (H3K36me3) (Larschan et al., 2007; Mukai et al., 2015; Stabell et al., 2007). H3K36me3 typically marks transcriptionally active genes (Bannister and Kouzarides, 2011; Dong and Weng, 2013; Keogh et al., 2005). How H3K36me3 regulates GSC differentiation is not clear. Interestingly, in male *Drosophila*, H3K36me3 facilitates recognition of the X chromosome by the Male-Specific Lethal (MSL) complex, which leads to hyper-transcription of the male X and gene dosage compensation with females, which have two X chromosomes (Bell et al., 2008; Conrad et al., 2012b; Larschan et al., 2007). Within the MSL complex, the chromodomain (CD) of MSL3 reads H3K36me3 marks and the histone acetyl transferase (HAT) Males absent on the first (MOF) deposits acetylation of histone H4 lysine 16 (H4K16ac) (Bone et al., 1994; Conrad et al., 2012a; Gu et al., 2000; Hilfiker et al., 1997; Larschan et al., 2007). Female flies do not

assemble the MSL complex because key components, including MSL2, are not expressed at sufficient levels (Bashaw and Baker, 1997; Kelley et al., 1997; UCHIDA et al., 1981). However, if individual MSL proteins in *Drosophila* regulate gene expression beyond their role in dosage compensation is not known.

Here, we find that Set2, MSL3, and a HAT complex, Ada2a-containing (ATAC), promote GSC differentiation. We discovered that MSL3 is expressed in the early stages of oogenesis, where it promotes the HAT-mediated transcription of several members of the SC as well as a germline-specific paralog of eukaryotic *Ribosomal protein S19* (*eRpS19*/*RpS19*). Expression of RpS19b (S19b) helps increase overall levels of RpS19, which is then required for translation of *Rbfox1* and thus promoting GSC differentiation into an oocyte.

Results

Set2 is required in the germline for proper differentiation

To determine how *Set2* promotes oogenesis in *Drosophila*, we stained control and *Set2* depleted fly gonads with antibodies against Vasa, a germline marker, and 1B1, a marker of somatic cell membranes, spectrosomes, and fusomes. Compared to controls, *Set2* depleted gonads displayed a loss spectrosome containing GSCs, an accumulation of fusome containing cysts, and a loss of proper egg chamber formation (**Fig. 1B-D; Fig. S1A-B'**). The *Set2* depleted germaria accumulated 8-, and 16 cell cysts as well cysts that were multinucleated upto 64 cells (n=30). The egg chambers that do form contain undifferentiated and differentiating cells marked by spectrosomes and fusomes that fail to develop further (100% in *Set2* RNAi compared to 0% in *nosGAL4*; $p<2.2E-16$, n=50), resulting in females that are infertile. Additionally, *Set2* depleted germ cells had significantly reduced H3K36me3 levels compared to the control, consistent with previous reports (Mukai et al., 2015) (**Fig. S1C-E**).

The accumulation of cyst-like structures upon germline depletion of *Set2* could be due to GSCs that divide but fail to undergo cytokinesis, resulting in GSC cysts, or differentiating cysts that cannot progress further in development (Carreira-Rosario et al., 2016; Mathieu and Huynh, 2017; Sanchez et al., 2016). To discern between these two types of cysts, we stained for pMad, a marker of GSCs. In addition, we crossed a *bam* transcriptional reporter, *bam-GFP*, into the Set2 RNAi background and independently assayed for Bam protein (Chen and McKearin, 2003b). We found that *Set2* RNAi germaria accumulated differentiating cysts, which transcribed and then translated Bam and were pMad negative (**Fig. 1E-F'; Fig. S1F-I'**). Thus, *Set2* is required in the germline downstream of *bam* to promote the differentiation of Bam expressing cysts into egg chambers.

Although germline depletion of *Set2* leads to both loss of GSCs and accumulation of cysts, here we focus on the cyst accumulation phenotype. Loss of *Set2* results in cysts that do not properly express the oocyte specific protein Orb (Mukai et al., 2015), but loss of Orb does not phenocopy loss of *Set2*, suggesting that Orb downregulation is a consequence of the differentiation defect (Barr et al., 2019; Christerson and McKearin, 1994; Huynh and St Johnston, 2000). Similar to loss of *Set2*, loss of Rbfox1 results in the accumulation of Bam expressing cysts that do not differentiate into proper egg chambers (Carreira-Rosario et al., 2016; Tastan et al., 2010). To test if *Set2* regulates Rbfox1 and Bru expression, we stained separately for Rbfox1 and Bru along with Vasa and 1B1 in control and germline *Set2* depleted ovaries. While control germaria express Rbfox1 robustly in 8-cell cysts, *Set2* depleted germ cells exhibited a significantly lower level of Rbfox1, while somatic levels were unchanged (**Fig. 1G-I**). Furthermore, Bru levels were reduced and enrichment to the oocyte was ablated in *Set2* RNAi germaria compared to controls (**Fig. S1J-L**). Thus, *Set2* is required after Bam expression to promote proper differentiation via Rbfox1 expression.

As germline depletion of *Set2* results in reduced levels of Rbfox1 and Bru, we hypothesized that *Set2* depleted cysts do not properly enter meiosis nor specify an oocyte. We stained control and *Set2* depleted germaria with antibodies against a SC member, Crossover suppressor on 3 of Gowen (C(3)G), and Vasa (Anderson et al., 2005; Page and Hawley, 2001). The control had several C(3)G positive germ cells in 16-cell cysts but only the most posterior germ cell in the egg chamber was marked with C(3)G. In *Set2* germline depleted germaria, the majority of cells displayed perturbed C(3)G expression; an irregular number of cells were C(3)G positive and C(3)G appeared fragmented (**Fig. 1J-K1'**). To determine if the oocyte is properly specified, we stained for the oocyte determinant Egalitarian (Egl), as well as Vasa and 1B1 (Carpenter, 1994; Huynh and St Johnston, 2000; Mach and Lehmann, 1997). While control 16-cell cysts had a single Egl positive cell, *Set2* germline depleted germaria showed diffuse staining of Egl without enrichment in a single cell (**Fig S1M-N'**). Thus, the H3K36me3 depositing enzyme Set2 is required for proper differentiation and oocyte specification.

MSL3 acts downstream of Set2 to promote proper differentiation independent of the MSL complex

To identify readers of H3K36me3 that activate transcription downstream of Set2, we screened 18 known Chromodomain (CD) containing proteins, which recognize lysine methylation marks, for loss of function phenotypes that phenocopied Set2 (Allis and Jenuwein, 2016; McCarthy et al., 2018; Navarro-Costa et al., 2016). Unexpectedly, of the 18 CD containing proteins that we examined by RNAi knockdown only MSL3 displayed a cyst accumulation phenotype (**Spread Sheet S1**). MSL3 is a reader of

H3K36me3 mark that promotes dosage compensation in the soma in male flies where it acts within the MSL complex in (Lucchesi and Kuroda, 2015), but whether MSL3 has a role in the female *Drosophila* germline has not been examined.

As a first test, we investigated MSL3 expression in ovaries. We analyzed *msl3* transcript levels at different stages of oogenesis, using RNA-seq libraries that we enriched for GSCs, CBs, cysts, and whole adult ovaries as previously described (McKearin and Ohlstein, 1995; Xie and Spradling, 1998; Zhang et al., 2014). We found that *msl3* mRNA is expressed during oogenesis consistent with what was reported on Flybase (THE MODENCODE CONSORTIUM et al., 2010)(**Fig. S2A**). We also examined ovaries from a fly line expressing GFP tagged MSL3 under endogenous control (Strukov et al., 2011), by staining for GFP and 1B1. We found that MSL3-GFP was expressed in the germline in single cells marked by spectrosomes and early cysts marked by fusomes (**Fig. 2A-A'; Fig. S2B**). Thus, unlike MSL2 (Bashaw and Baker, 1997; Parisi et al., 2001), MSL3 is expressed at appreciable levels during early stages of oogenesis at both the RNA and protein level.

To verify our RNAi knockdown experiments indicating a role in oogenesis, we examined validated *msl3* mutants (Bachiller and Sánchez, 1989; Sural et al., 2008; UCHIDA et al., 1981). As background mutations in *msl3* mutant stocks have been described to cause synthetic lethality (Erickson, 2016; Gladstein et al., 2010), we analyzed three independent alleles from different genetic backgrounds. We created trans-allelic combinations of independent *msl3* mutations to eliminate potential deleterious effects of homozygous background mutations; these combinations lead to cyst accumulation monitored by accumulation of fusome-positive cells, germline loss monitored by absence of Vasa-positive cells, and a reduction in formation of proper egg chambers (**Fig. 2B-D; Fig. S2C-D'**). Furthermore, as our screen indicated depletion of *msl3* in the germline alone using RNAi resulted in the accumulation of cysts, phenocopying *msl3* mutants (**Fig. 2D, Fig. S2E-F'**). The cysts that accumulate upon *msl3* germline depletion expressed *bam* but were pMad negative and failed to properly express Rbfox1 or Bru, phenocopying *Set2* germline depletion **(Fig. 2E-I; Fig. S2G-M).** In addition, these cysts failed to specify an oocyte, as monitored by Egl, and showed reduced expression of the synaptonemal protein C(3)G (**Fig. 2J-K1'; Fig. S2N-O'**). Lastly, expression of *msl3* in the germline of *msl3* mutant females was sufficient to rescue the differentiation defect (**Fig. 2L-M; Fig. 2D**). Taken together, we conclude that MSL3 is required in the female germline to promote proper differentiation.

To determine if the H3K36me3 writer Set2 and the H3K36me3 reader MSL3 act together to promote oogenesis, we generated flies heterozygous for *Set2* and *msl3*. While the trans-heterozygous flies were viable, the germaria of these trans-heterozygous flies displayed severe germline loss compared to single heterozygous controls (**Fig. S3A-C**). Although loss of MSL3 did not affect H3K36me3 levels, loss of *Set2* attenuated MSL3 expression (**Fig. S3D-H**). Together, these data suggest that Set2 and MSL3 impinge upon the same developmental pathway(s), with MSL3 acting downstream of Set2 to promote proper differentiation.

This function of MSL3 during oogenesis is independent of its role in the MSL complex as we found that *msl2*, *roX1,* and *roX2* are barely expressed (<1 TPM), consistent with previous reports (Bashaw and Baker, 1997; Meller et al., 1997; Parisi et al., 2004). Additionally, validated *msl1*, *msl2*, and *mle* mutants (Bachiller and Sánchez, 1989; Belote, 1983; UCHIDA et al., 1981) did not result in early oogenesis defects (**Fig. S3I**) nor did loss of germline MOF (Sun et al., 2015).

ATAC complex acts with Set2 and MSL3 to promote proper differentiation

We asked if the H3K36me3 reader MSL3 cooperates with another HAT-containing complex to regulate cyst differentiation. Using an RNAi screen, we found that members of the Ada2a-containing (ATAC) complex phenocopy loss of *Set2* and *msl3* in the germline (McCarthy et al., 2018; Spedale et al., 2012; Suganuma et al., 2008) (**Fig. 3A-C; Fig. S4A-H)**. The ATAC complex contains thirteen proteins some shared with other complexes, including Gcn5 (Spedale et al., 2012). Depletion of six members, four of which are specific to the ATAC complex, resulted in the accumulation of cysts and germline loss (**Fig. S4A-H**) Of these ATAC complex members, we chose to focus on Negative Cofactor 2β (NC2β), as its defect was highly penetrant but maintained sufficient germline for transcriptomic analysis.

Loss of NC2β in the germline led to GSC loss monitored by loss of spectrosome containing cells and accumulation of cysts-like structures that were marked by fusomes (**Fig. 3A-C; Fig. S4A-B'**). To determine if the cysts that accumulate due to loss of *NC2β* phenocopy cysts that accumulate due to loss of *Set2* and *msl3*, we independently probed for GSC marker pMad and differentiation markers Bam, Rbfox1 and Bru. In addition, we also probed for meiotic marker C(3)G. We found that cysts that accumulate upon germline depletion of NC2β expressed Bam, did not contain pMad positive cells or properly express Rbfox1 or Bru (**Fig. 3D-H; Fig. S5A-G**). In addition, loss of *NC2β* leads to meiotic defects and oocyte specification as monitored by C(3)G localization and Egl respectively (**Fig. 3I-J1'; Fig. S5H-I'**). These data suggest that the ATAC complex, is required for proper differentiation as well as oocyte specification phenocopying loss of *Set2* and *msl3*.

As components of the ATAC complex phenocopy loss of the H3K36me3 writer *Set2* and the H3K36me3 reader *msl3*, we asked whether the ATAC complex acts downstream of H3K36me3 mark to promote proper meiosis. To test this, we stained for H3K36me3 in *NC2β* RNAi flies and found that H3K36me3 levels were unaltered suggesting that ATAC complex acts downstream of *Set2* (**Fig. S5J-L**). In addition, we made use of a mutant of the active HAT in the ATAC complex, Atac2, as there were no *NC2β* mutants available. We generated flies heterozygous for both *Atac2* and *msl3* and found that while trans-heterozygotes flies were viable their germaria had severe defects compared to controls (**Fig. S5M-O**). Thus, the ATAC complex works downstream of Set2, and *Atac2* genetically interacts with *msl3*. Taken together, our data suggest that Set2, MSL3, and ATAC complex impinge upon the same developmental pathway(s) to regulate differentiation in the *Drosophila* female germline.

Set2, MSL3, and NC2β promote transcription of the ribosomal protein paralog *RpS19b*

To determine how Set2, MSL3, and ATAC promote differention, we compared the transcriptomes of *Set2*, *msl3*, and *NC2β* germline depleted ovaries to a developmental control that accumulates cysts. To enrich for cysts we induced *bam* expression under control of a *heat-shock* (*hs*) promoter in the background of germaria depleted for *bam* (*bam* RNAi;*hs-bam*) (Ohlstein and McKearin, 1997; Zhang et al., 2014). We found 662 significantly downregulated and 65 significantly upregulated RNAs in *Set2* depleted germaria compared to *bam* RNAi;*hs-bam* ovaries (Fold Change >|4|; False discovery rate (FDR)<0.05) (**Fig. 4A**). There were 283 significantly downregulated RNAs and 302 significantly upregulated RNAs in *msl3* RNAi compared to *bam* RNAi;*hs-bam* (**Fig. 4A'**). Lastly, there were 466 RNAs significantly downregulated and 277 upregulated, in *NC2β* RNAi compared to the developmental control (**Fig. 4A''**). Set2 and ATAC are part of the generalized transcriptional machinery and are expected to regulate more genes than MSL3 alone. This is evident in the RNA-seq results where we find more downregulated targets upon the loss of *Set2* (662) and *NC2β* (466) than loss of *msl3* (283) (**Fig. 4A-A''**). Of those transcripts that were differentially expressed in *Set2*, *msl3*, and *NC2β* depleted germ cells compared to *bam* RNAi; *hs-bam* control there were 29 shared RNAs that were downregulated (**Fig. 4B**) and 11 shared RNAs that were upregulated (**Spread Sheet S2**). This small but significant overlap of targets suggests a specific subset of Msl3 targets are co-regulated by Set2 and ATAC.

Although Rbfox1 protein is not properly expressed upon loss of Set2, MSL3, and NC2β, *Rbfox1* mRNA was not among the shared downregulated RNAs (**Fig. 4C**). We verified that *Rbfox1* mRNA was present in the germline of *msl3* depleted ovaries by *in situ* hybridization (**Fig. S6A-B'**). Thus, Set2, MSL3, and ATAC do not regulate *Rbfox1* mRNA levels to promote differentiation. In contrast, we found that several SC member genes were among the shared downregulated genes, including *orientation disruptor*

(*ord*), *sisters unbound* (*sunn*), and *corona* (*cona*) (Hughes et al., 2018) but C(3)G was not among those genes (**Fig. 4D-E; Fig. S6C-D**). To validate the loss of SC components, we crossed an Ord-GFP line that is under endogenous control (Balicky et al., 2002) into *msl3* mutants and found that *msl3* mutant ovaries had both lower levels and an altered location of Ord-GFP compared to controls (**Fig. S6E-F'**). While this change can be mediated by both RNA levels or protein stability, we found ord nascent mRNAs levels are also downregulated (see below). The shared downregulated targets also included 11 candidate genes (CGs) of unknown function, and the ribosomal protein paralog, *RpS19b* (*S19b*), but not *RpS19a* (*S19a*) (**Fig. 4B, F; Fig. S6G-J'**).

We hypothesized that MSL3 and MSL3-regulated mRNAs would be expressed at the same stages, from GSCs until the cyst stages. To test this hypothesis, we analyzed mRNA levels of the 29 targets in RNA-seq libraries enriched for either GSCs, CBs, cysts, or unenriched wild type ovaries. Indeed, transcript levels overlap with MSL3 expression and then dropped off (**Fig. 4G**). Lastly, to determine if SC genes and *RpS19b* were affected at the level of transcription, we measured nascent mRNA (pre-mRNA) levels utilizing qRT-PCR as a proxy for transcription. We found that upon depletion of *msl3*, nascent mRNA levels of SC genes and RpS19b are significantly lower (**Fig. 4H**). Taken together, these data suggest that Set2, MSL3, and ATAC regulate transcription of SC components and *RpS19b,* but not *Rbfox1*, during differentiation. While loss of SC components leads to loss of recombination, it does not cause a differentiation defect (Collins et al., 2014b). Proper cyst differentiation is mediated by Rbfox1 (Carreira-Rosario et al., 2016; Tastan et al., 2010). Altogether, this suggests that a target of Set2, MSL3, and ATAC regulates not *Rbfox1* mRNA levels but another aspect of the protein's expression, potentially its translation to promote differentiation.

RpS19b is a germline enriched ribosomal protein required for Rbfox1 translation

RpS19b is a ribosomal protein and is one of two RpS19 paralogs in *Drosophila.* Given that loss of Set2, MSL3, and NC2β decreased Rbfox1 protein levels without affecting *Rbfox1* mRNA levels, we hypothesized that the reduced RpS19b expression we observed in these mutants resulted in the decreased translation of *Rbfox1* mRNA. If RpS19b is required for Rbfox1 translation, then the RpS19b protein should be present when Rbfox1 protein expression occurs. We examined lines expressing RpS19b-GFP and RpS19a-HA from under endogenous control. RpS19b-GFP was germline enriched while RpS19a-HA was expressed in both the germline and soma of the gonad (**Fig. 5A-A1; Fig. S7A-B**). In the germline, RpS19b-GFP was expressed at high levels in single cells and gradually decreased in cyst stages, which overlapped with the protein expression of MSL3 and Rbfox1 (**Fig. 5B**).

If RpS19b acts downstream of MSL3 to promote the translation of *Rbfox1* mRNA, then loss of RpS19b should result in reduced Rbfox1 protein levels and a germline phenotype that phenocopies that of *msl3*. We used RNAi to specifically deplete *RpS19b* but not *RpS19a* in the germline (**Fig. S7C-F'**) and found that *RpS19b* depleted germaria accumulated *bam* positive cysts that lack Rbfox1 protein (**Fig. 5C-H; Fig. S7G-H'**). To test if *RpS19b* is one of the main targets of *msl3* we asked whether the addition of *RpS19b* could rescue the differentiation defect of *msl3* mutants. Adding one copy of *RpS19b-GFP* in *msl3* mutant flies rescued the early cyst defect, including Rbfox1 expression, and led to egg chamber formation (**Fig. 5I-M**). Overexpression of *RpS19b* could also rescue the differentiation defect upon germline depletion of *msl3,* leading to egg chamber formation (**Fig. 5N-O**). Thus, our data suggest that MSL3 promotes the expression of RpS19b and thus *Rbfox1* translation and proper differentiation.

Our model predicts that the MSL3-mediated transcription of the SC members *ord*, *sunn* and *cona* is independent of Rbfox1 protein expression. To test this model, we examined the localization of the SC component C(3)G in *msl3* mutants that express RpS19b (Anderson et al., 2005; Page and Hawley, 2001). C(3)G was not a coregulated target and thus allowed us to visualize SC defects. We found that while *msl3* mutants with restored RpS19b expression make egg chambers, C(3)G does not properly localize to the oocyte nucleus in egg chambers and the females were infertile (**Fig. 5P-Q'**). Thus, RpS19b is not involved in MSL3-mediated transcriptional regulation of SC members to promote recombination during meiosis.

RpS19 levels, not paralog specificity, are critical for proper differentiation

To validate the role of RpS19b in oogenesis, we generated a CRISPR null mutant of the gene ($RpS19b^{CRISPR}$). This null is viable but unexpectedly did not display any oogenesis defects in contrast to *RpS19b* RNAi (**Fig. S7I-K**). Studies in organisms including zebrafish have reported transcriptional compensation in mutants, but not upon depletion by RNAi (El-Brolosy et al., 2019). To determine if the $RpS19b^{CRISPR}$ mutants display transcriptional changes, we performed RNA-seq of CB enriched ovaries from control and $RpS19b^{CRISPR}$ flies, both with a *bam* depleted background to enrich for the undifferentiated stages in which *RpS19b* is primarily expressed. We found that loss of *RpS19b* resulted in 79 downregulated genes and 934 upregulated genes with 9-fold downregulation of *RpS19b* but no increase in *RpS19a* RNA levels (**Fig. S7L**). As RpS19a mRNA levels were not altered, we then asked if *RpS19b* mutants have proper development because they have increased levels of RpS19a protein. Using an RpS19 antibody that detects both paralogs, we found that levels of RpS19 were not downregulated in $RpS19b^{CRISPR}$ mutant gonads compared to the control (**Fig. S7M-P**). Furthermore, germline depletion of *RpS19a* in $RpS19b^{CRISPR}$ mutants results in the complete loss of the germline, while there is no defect at all in homozygous

RpS19b^{CRISPR} mutants and only the accumulation of cysts upon *RpS19a* depletion alone (**Fig. S7Q-R**). In contrast, *RpS19b* depletion in *RpS19b*^{CRISPR} mutants resulted in no defect (**Fig. S7S-T**). Thus, we conclude that full loss of RpS19b can be compensated by increased levels of RpS19a in *RpS19b*^{CRISPR} but not in *RpS19b* RNAi, via as yet unknown mechanisms.

This data suggests that what is required for Rbfox1 translation is a critical level of RpS19, which can be provided by either the RpS19a or S19b isoforms or a combination of both. To test this, we depleted *RpS19a* from the germline and found that the germaria accumulate *bam* positive cysts that have significantly reduced levels of Rbfox1 (**Fig. S8A-L'**). Ectopic expression of RpS19a-HA in *msl3* depleted ovaries that have reduced levels of RpS19b restored Rbfox1 protein expression and egg chamber formation (**Fig. S8M-P)**. Consistent with our previous data showing that Rps19b cannot rescue expression of SC components in the *msl3* mutant, these females were also infertile and had perturbed C(3)G localization (**Fig. S8Q-R**). Furthermore, expression of human RpS19 in the germline of *msl3* depleted germaria also was able to rescue the cyst accumulation phenotype, leading to the production of normal egg chambers (**Fig. S8S-T1**). Thus, our data taken together suggests that proper dosage of RpS19 is essential for the translation of Rbfox1 protein.

RpS19 promotes *Rbfox1* translation in the germline

We next examined the requirement for RpS19 in Rbfox1 translation. First, to determine if RpS19a and S19b were incorporated into actively translating ribosomes, we performed polysome profiling followed by western blot analysis using wild type ovaries and those enriched for undifferentiated germ cell cysts (*bam* RNAi). While RpS19a-HA is present in polysome fractions in wild type ovaries, RpS19b-GFP appears to be preferentially enriched in polysomes from ovaries enriched for undifferentiated germ cells consistent with its expression pattern early in oogenesis (**Fig. 6A-B'**). To test if RpS19 paralogs affect translation in cysts, we pulsed gonads with a puromycin analog, O-propargyl-puromycin (OPP), that is incorporated into translated peptides and can be detected using Click-chemistry (Sanchez et al., 2016). We found that cysts that accumulate upon the loss of RpS19a and RpS19b have decreased translation compared to cysts of control ovaries (**Fig. 6C-F**). Thus, we find that RpS19a and S19b are present in the translating polysomes and are important for translation in cysts.

To directly test whether RpS19b is required for *Rbfox1* translation specifically we then performed polysome-seq on germaria depleted of *RpS19b* compared to control germaria enriched for cysts using *bam RNAi*;*hs-bam* (**Fig. 6G-H**). Depletion of germline *RpS19b* did not significantly affect the translation of the germline specific mRNA, *nanos,* but there was a reduction in *Rbfox1* cytoplasmic isoform mRNA translation, compared

to the control (**Fig. 6I-J**). Additionally, depletion of *RpS19b* using RNAi, did not reduce the levels or translation efficiency of *RpS19a* (**Fig. 6K**). Taken together, our data suggest that there is an increased expression of RpS19 during early development that is required for translation of *Rbfox1* mRNA.

Discussion

We have identified Set2, MSL3, and the ATAC complex as transcriptional regulators of differentiation and proper meiosis in *Drosophila*. We find that Set2, MSL3, and ATAC together regulate oogenesis downstream of the differentiation factor, Bam, but upstream of the critical differentiation factor, Rbfox1. While we find significant shared targets between Set2, MSL3, and NC2β that control differentiation, the total number of shared targets is small. One reason for this could be MSL3's ability to also read H4K20me1 marks (Kim et al., 2010), allowing it to affect a distinct set of targets than those marked by the H3K36me3 laid down by Set2. Similarly, MSL3 could recruit a different HAT than the one associated with NC2β, one that functions in the undifferentiated stages (McCarthy et al., 2018). Thus, we hypothesize that Set2, MSL3, and ATAC work in concert on a select subset of targets to regulate meiosis and oogenesis.

We find that temporally specific recruitment by MSL3 of the basal transcriptional machinery, ATAC to the Set2 mediated H3K36me3 marks would lead to enhanced transcription of a subset of genes that promote differentiation at the proper stage. We do not know what controls the expression of MSL3 itself during oogenesis. *msl3* mRNA is present as part of the maternal contribution deposited into the developing oocyte (Eichhorn et al., 2016; Hua et al., 2014) This suggests that *msl3* mRNA is also transcribed in the later stages of oogenesis and is likely post-transcriptionally regulated in the later stages. While our data demonstrates that MSL3 expression is required for proper differentiation in female *Drosophila*, we do not think MSL3 expression is sufficient for differentiation as overexpression of *msl3* does not lead to precocious differentiation (**Fig. 2L-M**).

We find that Set2, MSL3, and ATAC regulate oogenesis in two ways: 1) they transcriptionally upregulate members of the synaptonemal complex that are critical for recombination and 2) they promote transcription of the germline enriched *RpS19* paralog, *RpS19b*. The expression of RpS19b then controls the translation of *Rbfox1*, which is required for exit from the mitotic cell cycle and entry into the meiotic cell cycle (**Fig. 7**). While several components of the synaptonemal complex, Cona, Ord, and Sunn, are regulated at the transcriptional level by Set2, MSL3 and ATAC, components such as C(3)G and Crossover suppressor on 2 of Manheim (C(2)M) are not. This

suggests that some synaptonemal complex members such as C(2)M and C(3)G may be regulated at the post-transcriptional level. Taken together, this data argues that the Set2-MSL3-ATAC complex coordinates the transcription of several critical factors of the recombination machinery and the translation of a meiotic cell cycle regulator to promote proper oogenesis (**Fig. 7**).

Acknowledgments
We are grateful to Drs. Marlow and Siekhaus for comments. We would like to thank Drs. Kuroda, Bach, Lehmann, Hawley, Bickel, Fuchs for reagents. We thank Bloomington, Vienna Drosophila Resource Center and Transgenic RNAi Project (NIH/NIGMS R01-GM084947) for fly stocks. P.R. is funded by National Institutes of Health 2R01GM111770–06 and RO1GM135628, M.B. by R01GM125812 and P.F. by 1R15HD0964110, 1R01HD097331-01 and 1R01DC017149-01A1.

Contributions
A.M., K.S., P.F., M.U., and P.R. designed experiments, analyzed, and interpreted data. E.T.M. provided bioinformatic support. N.D.M., S.J., and M.B. made RpS19a and RpS19b fly lines. A.M. and P.R. wrote the manuscript, which all authors edited and approved.

Declaration of Interests
The authors declare no competing interests.

Materials and Methods

Fly lines

Flies were grown at 25-31°C and dissected between 1-5 days post-eclosion.

The following RNAi stocks were used in this study; if more than one line is listed, then both were quantitated and the first was shown in the main figure: *Set2* RNAi (Bloomington #33706 (#1) and #42511 (#2)), *msl3* RNAi (Bloomington #35272), *NC2β* RNAi (Bloomington #57421 (#1) and VDRC #v3161 (#2)), *Ada2a* RNAi (Bloomington #50905), *Atac1* RNAi (VDRC #v36092), *Atac2* RNAi (VDRC #v16047), *D12* RNAi (VDRC #v29954), *wds* RNAi (Bloomington #60399), *NC2α* RNAi (Bloomington #67277), *bam* RNAi (Bloomington #58178), *hs-bam*/TM3 (Bloomington #24637) *RpS19b* RNAi (VDRC #v22073 and #v102171), and *RpS19a* RNAi (Bloomington #42774 and VDRC #v107188).

The following mutant and overexpression stocks were used in this study: *Set2*^{1}/FM7 (Bloomington #77916), *msl3*^{1}/TM3 (Bloomington #5872), *msl3*^{KG}/TM3 (Bloomington #13165), *mls3*^{MB}/TM3 (Bloomington #29244), *msl1*^{v216}/CyO (Bloomington #5870), *msl1*^{kmB}/CyO (Bloomington #25157), *msl2*^{227}/CyO (Bloomington #5871), *msl2*^{kmA}/CyO (Bloomington #25158), *mle*^{1}/SM1 (Bloomington #4235), *mle*^{9}/CyO (Bloomington #5873), *Hel89B*^{08724}/TM3 (Bloomington #11732), *Hel89B Df*/TM6 (Bloomington #7982), *Atac2*^{e03046}/CyO (Bloomington #18111), *RpS19b*^{EY00801} (Bloomington #15043), *RpS19b*^{CRISPR} (this study), *UAS-hRpS19-HA* (Bloomington #66014), and *UAS-msl3-GFP* (this study).

The following tagged lines were used in this study: *msl3-GFP* (Kuroda Lab), *RpS19a-3xHA* (this study), *RpS19b-GFP* (this study), and *ord-GFP* (Bickel Lab).

The following tissue-specific drivers were used in this study: *UAS-Dcr2;nosGAL4* (Bloomington #25751), *UAS-Dcr2;nosGAL4;bam-GFP* (Lehmann Lab) and *If*/CyO*;nosGAL4* (Lehmann Lab). We used *UAS-Dcr2;nosGAL4* for all RNAi experiments as this combination as it gave us the most consistent phenotype with most germline in all genotypes indicated.

Dissection and Immunostaining

Ovaries were dissected and stained as previously described (McCarthy et al., 2018). The following primary antibodies were used: mouse anti-1B1 (1:20; DSHB), Rabbit anti-Vasa (1:1,000; Rangan Lab), Chicken anti-Vasa (1:1,000 (Upadhyay et al., 2016)), Rabbit anti-GFP (1:2,000; abcam, ab6556), Guinea pig anti-Rbfox1 (1:1,000 (Tastan et al., 2010)), Mouse anti-C(3)G (1:1000; Hawley Lab), Rabbit anti-H3K36me3 (1:500; abcam, ab9050), Rabbit anti-pMAD (1:150; abcam, ab52903), Mouse anti-BamC (1:200; DSHB, Supernatant), Rabbit anti-Bru (1:500; Lehmann Lab), Rabbit anti-Egl (1:1,000; Lehmann Lab), Rat anti-HA (1:500; Roche, 11 867 423 001), and Rabbit anti-RpS19 (1:20; Proteintech, 15085-1-AP). Anti-RpS19 was pre-cleared at 1:20, the supernatant was then diluted at 1:2.5 for staining. The following secondary antibodies were used: Alexa 488 (Molecular Probes), Cy3 and Cy5 (Jackson Labs) were used at a dilution of 1:500.

Fluorescence Imaging

The tissues were visualized, and images were acquired using a Zeiss LSM-710 confocal microscope under 20X, 40X and 63X oil objective.

Quantification of phenotypes

We quantified loss of germline by counting ovarioles that did not have vasa positive cells. For loss of stem cells, we quantified loss of spectrosome containing cells. For cyst differentiation defect, we counted the number of germaria with cysts with >16 cells and/or accumulation of 16-cell cysts close to the niche.

AU quantification of protein or *in situ*

To quantify antibody staining intensities for Rbfox1, H3K36me3, Bruno, GFP, HA, and RpS19 or *in situ* probe fluorescence in germ cells, images for both control and experimental germaria were taken using the same confocal settings. Z stacks were obtained for all images. Similar planes in control and experimental germaria were chosen, the area of germ cells positive for the proteins or *in situs* of interest was outlined and analyzed using the 'analyze' tool in Fiji (ImageJ). The mean intensity and area of the specified region was obtained. An average of all the ratios (Mean/Area), for the proteins or *in situs* of interest, per image was calculated for both, control and experimental. Germline intensities were normalized to somatic intensities or if the protein or *in situ* of interest is germline enriched and not expressed in the soma they were normalized to Vasa or background. The highest mean intensity between control and experimental(s) was used to normalize to a value of 1 A.U. on the graph. A minimum of 5 germaria was used for quantitation.

Egg laying assays

Assays were conducted in cages with females under testing and wild type control males. Cages were maintained at 25°C. All flies were 1 day post-eclosion upon setting up the experiment and analyses were performed on four consecutive days. The number of eggs laid were normalized to the total number of females.

RNA-seq library preparation and analysis

Ovaries from flies of various genotypes were dissected in 1x PBS. For enriching GSCs, we over overexpressed TKV in the germline, for CBs, we used *bam* mutant and for cysts we used *bam* mutant also carrying *hsbam* trangene. Post heat-shock CBs converted to cysts. RNA was isolated using TRIzol (Invitrogen, 15596026), treated with DNase (TURBO DNA-free Kit, Life Technologies, AM1907), and then run on a 1% agarose gel to check integrity of the RNA. To generate mRNA enriched libraries, total RNA was treated with poly(A)tail selection beads (Bioo Scientific Corp., NOVA-512991) and then following the manufacturer's instructions of the NEXTflex Rapid Directional RNA-seq Kit (Bioo Scientific Corp., NOVA-5138-08), except that RNA was fragmented for 13 min. Single-end mRNA sequencing (75 base pair) was performed on biological duplicates from each genotype on an Illumina NextSeq500 by the Center for Functional Genomics (CFG).

After quality assessment, the sequenced reads were aligned to the *Drosophila melanogaster* genome (UCSCdm6) using HISAT2 (version 2.1.0) with the RefSeq-annotated transcripts as a guide (Kim et al., 2015). Raw counts were generated using featureCounts (version 1.6.0.4) (Liao et al., 2014). Differential gene expression was assayed by edgeR (version 3.16.5), using a false discovery rate (FDR) of 0.05, and genes with fourfold or higher were considered significant. The raw and unprocessed data for RNA-seq generated during this study are available at Gene Expression Omnibus (GEO) databank under accession number: GSE143728.

In situ hybridization

Adult ovaries (5 ovary pairs per sample per experiment) were dissected and fixed as previously described. The ovaries were washed with PT (1x phosphate-buffered saline (PBS), 0.1% Triton-X 100) 3 times for 5 minutes each. Ovaries were permeabilized by washing once with increasing concentrations of methanol for 5 minutes each (30% methanol in PT, 50% methanol in PT, and 70% methanol in PT) then incubating in methanol for 10 minutes. Ovaries were then post-fixed by washing once with decreasing concentrations of methanol for 5 minutes each (70% methanol in PT, 50% methanol in PT, and 30% methanol in PT). Ovaries were then washed with PT 3 times for 5 minutes and then pre-hybridized in wash buffer for 10 minutes (10% deionized formamide and 10% 20x SSC in RNase-free water). Ovaries were incubated overnight in hybridization solution (10% dextran sulfate, 1 mg/ml yeast tRNA, 2 mM RNaseOUT, 0.02 mg/ml BSA, 5x SSC, 10% deionized formamide, and RNase-free water) at 30°C. The hybridization solution was removed, and ovaries washed with Wash Buffer 2 times for 30 minutes at 30°C. Wash Buffer was removed, and ovaries were mounted using Vectashield with 4’,6’-diamidino-2-phenylindole (DAPI).

In situ probe design and generation

Templates were amplified with gene specific primers (listed below) and then followed manufacturer’s instructions of Thermo Fisher’s FISH tag RNA kit (F32954) for generating fluorescently labeled probes.

Rbfox1
F- 5’-CGTAGCGCCTTTTCCGGG-3’
R- 5’-TAATACGACTCACTATAGGGCCACAGCCGCCACTTGAATA-3’

RpS19b
F- 5’-TGCCTGGAGTCACAGTAAAGG-3’
R- 5’-TAATACGACTCACTATAGGGTGTTGGCTATGCGATCCAAGT-3’

RpS19a
F- 5'-ATGCCAGGCGTCACAGTGAA-3'
R- 5'-TAATACGACTCACTATAGGGTTACTTGGAAATAACAATGGGCCC-3'

Measurement of global protein synthesis

Protein synthesis was detected using short-term ovary incorporation assay, Click-iT Plus OPP (Invitrogen, C10456). Ovaries were dissected in Schneider's *Drosophila* media (Thermo Fisher, 21720024) and then incubated in 50 μM OPP reagent for 30 minutes. Tissue was washed in 1x PBS and then fixed for 15 min in 1x PBS plus 5% methanol-free formaldehyde. Tissue was then permeabilized with 1% Triton X-100 in 1x PBST (1x PBS with 0.2% Tween 20) for 30 minutes, samples were then washed in 1x PBS and were incubated in Click-iT reaction cocktail following the manufacturer's instructions. Samples were washed with Click-iT reaction rise buffer and then immunostained following previously described procedures.

Generating fly lines

CRISPR mutant

To generate the *RpS19b* mutants, guide RNAs were designed using http://tools.flycrispr.molbio.wisc.edu/targetFinder and synthesized as 5-unphosphorylated oligonucleotides, annealed, phosphorylated, and ligated into the BbsI sites of the pU6-BbsI-chiRNA vector using the primers listed below (Gratz et al., 2013). Homology arms were synthesized as a gene block (IDTDNA) and cloned into pHD-dsRed-attP ((Gratz et al., 2015); Addgene) using Gibson Assembly (gene blocks listed in Supplementary Methods). Guide RNAs and the donor vector were co-injected into *nos-Cas9* embryos (Rainbow Transgenics).

RpS19b gRNA1
F- 5'-CTTCGCATGCCTGGAGTCACAGTAA-3'
R- 5'-AAACTTACTGTGACTCCAGGCATGC-3'

RpS19b gRNA2
F- 5'-CTTCGTAGTGATAATCATGGAAAC-3'
R- 5'-AAACGTTTCCATGATTATCACTAC-3'

***RpS19a-3xHA* and *RpS19b-GFP* tagged lines**

RpS19a3x-HA (referred to as *RpS19a-HA* throughout text) and *RpS19b-GFP* tagged lines were made using a combination of *in vivo* bacterial recombineering and GatewayTM Technology as previously described (Shalaby et al., 2017).

***UAS-msl3-GFP* overexpression line**

RNA was extracted from w^{1118} ovaries and made into cDNA using a SuperScript II-Strand Kit (Thermo Fisher, 18064014). *msl3* CDS was amplified, *att*B sites and tagged sequence was amplified into the PCR product using the primers listed below. PCR products were cloned into pDONR (Thermo Fisher, 11789-020) and swapped into pENTR (Thermo Fisher, 11791-020) using BP and LR reactions, respectively. The plasmid was sent for injection into w^{1118} flies (Genetic Services).

msl3 CDS
F- 5'- ATGACGGAGCTAAGGGACGAGAC-3'
R- 5'- CTAAGCAGCAATCCCATCCAGGG-3'

*att*B
F-5'-GGGGACAAGTTTGTACAAAAAAGCAGGCTTCATGACGGAGCT
AAGGGACGAGAC-3'
R-5'-GGGGACCACTTTGTACAAGAAAGCTGGGTCCTAAGCGTAATC
TGGCACATCGTATGGGTAAGCAGCAATCCCATCCAGGG -3'

Polysome profiling and polysome-seq

Polysome profiling of ovaries from *bam* RNAi*;hs-bam* and *UAS-Dcr2;nosGAL4 >RpS19b* RNAi flies was adapted from (Flora et al., 2018; Fuchs et al., 2011). 200 ovary pairs were dissected in Schneider's media and immediately flash frozen with liquid nitrogen. Ovaries were homogenized in Lysis Buffer, 20% of lysate was used as input for mRNA isolation and library preparation (as described above). Samples were loaded onto 10-50% CHX-supplemented sucrose gradients in 9/16 x 3.5 PA tubes (Beckman Coulter, #331372) and spun at 35,000 x g in SW41 for 2.45-3 hours at 4°C. Gradients were fractionated with a Density Gradient Fractionation System (#621140007). RNA was extracted using acid phenol-chloroform and precipitated overnight. Pelleted RNA was resuspended in 20 µL water and libraries were prepared as described above.

Western blot

50-200 CB enriched *RpS19b-GFP* ovaries and 30 adult *RpS19b-GFP;RpS19a-HA* ovaries were dissected and prepared as described above except sucrose solutions were supplemented with either 100 µg/µL CHX or 2 mM puromycin with 1 mg heparin prior to making gradients. Following fractionation, protein was extracted by ethanol precipitation and run on a TGX pre-cast gradient gel (BioRad, #456-1094). Blots were blocked with 5% milk in 1x PBST and incubated in primary antibody in 5% BSA in 1x PBST. Following 1x PBST washing, blots were incubated in secondary antibody in 5% milk in 1x PBST. Blots were washed with 1x PBST and then imaged with chemi-luminescence kit (BioRad, #170-5060). The following primary antibodies were used:

Rabbit anti-GFP (1:4,000; abcam, ab6556), Rat anti-HA (1:3,000; Roche, 11 867 423 001), Rabbit anti-RpS25 (1:1,000; abcam, ab40820), and Rabbit anti-RpS19 (1:1,000; Proteintech, 15085-1-AP). The following secondary antibodies were used: anti-Rat HRP (1:10,000; Jackson Labs, 112-035-003) and anti-Rabbit HRP (1:10,000; Jackson Labs, 111-035-144).

Statistical Analysis

Relative fluorescence signals were compared between control and experimental groups using parametric tests (Student t-test or one-way ANOVA). Horizontal lines on scatter dot plots represent mean with 95% confidence interval and stars on stacked bar graphs represent statistical significance of corresponding color data set. Reported p-values correspond to two-tailed tests. Analysis of percentage defect were compared between control and experimental groups using Fisher's exact test. All analyses were performed using Prism 8 software (GraphPad) and reported in figure legends.

Materials and reagents for fly husbandry

Fly food was made by using previously described procedures (Upadhyay et al., 2018).

References

Ables, Elizabeth T., 2015. Drosophila Oocytes as a Model for Understanding Meiosis: An Educational Primer to Accompany "Corolla Is a Novel Protein That Contributes to the Architecture of the Synaptonemal Complex of Drosophila." Genetics 199, 17–23. https://doi.org/10.1534/genetics.114.167940

Ables, Elizabeth T, 2015. Drosophila Oocytes as a Model for Understanding Meiosis: An Educational Primer to Accompany "Corolla Is a Novel Protein That Contributes to the Architecture of the Synaptonemal Complex of Drosophila." Genetics 199, 17 LP – 23. https://doi.org/10.1534/genetics.114.167940

Allis, C.D., Jenuwein, T., 2016. The molecular hallmarks of epigenetic control. Nature Reviews Genetics 17, 487. https://doi.org/10.1038/nrg.2016.59

Anderson, L.K., Royer, S.M., Page, S.L., McKim, K.S., Lai, A., Lilly, M.A., Hawley, R.S., 2005. Juxtaposition of C(2)M and the transverse filament protein C(3)G within the central region of Drosophila synaptonemal complex. Proceedings of the National Academy of Sciences of the United States of America 102, 4482–4487.

Bachiller, D., Sánchez, L., 1989. Further analysis on the male-specific lethal mutations that affect dosage compensation in Drosophila melanogaster. Roux's Archives of Developmental Biology 198, 34–38. https://doi.org/10.1007/BF00376368

Balicky, E.M., Endres, M.W., Lai, C., Bickel, S.E., 2002. Meiotic cohesion requires accumulation of ORD on chromosomes before condensation. Molecular biology of the cell 13, 3890–3900.

Bannister, A.J., Kouzarides, T., 2011. Regulation of chromatin by histone modifications. Cell Research. https://doi.org/10.1038/cr.2011.22

Bannister, A.J., Zegerman, P., Partridge, J.F., Miska, E.A., Thomas, J.O., Allshire, R.C., Kouzarides, T., 2001. Selective recognition of methylated lysine 9 on histone H3 by the HP1 chromo domain. Nature 410, 120–124. https://doi.org/10.1038/35065138

Barr, J., Charania, S., Gilmutdinov, R., Yakovlev, K., Shidlovskii, Y., Schedl, P., 2019. The CPEB translational regulator, Orb, functions together with Par proteins to polarize the Drosophila oocyte. PLOS Genetics 15, e1008012.
Bashaw, G.J., Baker, B.S., 1997. The regulation of the Drosophila msl-2 gene reveals a function for Sex-lethal in translational control. Cell 89, 789–798.
Bell, O., Conrad, T., Kind, J., Wirbelauer, C., Akhtar, A., Schubeler, D., Schübeler, D., 2008. Transcription-Coupled Methylation of Histone H3 at Lysine 36 Regulates Dosage Compensation by Enhancing Recruitment of the MSL Complex in Drosophila melanogaster. Molecular and Cellular Biology 28, 3401–3409. https://doi.org/10.1128/mcb.00006-08
Belote, J.M., 1983. Male-Specific Lethal Mutations of DROSOPHILA MELANOGASTER . II. Parameters of Gene Action during Male Development. Genetics 105, 881–896.
Belote, J.M., Lucchesi, J.C., 1980. Male-specific lethal mutations of Drosophila melanogaster. Genetics 96, 165–186.
Bone, J.R., Lavender, J., Richman, R., Palmer, M.J., Turner, B.M., Kuroda, M.I., 1994. Acetylated histone H4 on the male X chromosome is associated with dosage compensation in Drosophila. Genes & development 8, 96–104.
Carpenter, A.T., 1994. Egalitarian and the choice of cell fates in Drosophila melanogaster oogenesis. Ciba Foundation symposium 182, 223-46-discussion 246-54.
Carpenter, A.T., 1975. Electron microscopy of meiosis in Drosophila melanogaster females. I. Structure, arrangement, and temporal change of the synaptonemal complex in wild-type. Chromosoma 51, 157–182.
Carpenter, A.T., Sandler, L., 1974. On recombination-defective meiotic mutants in Drosophila melanogaster. Genetics 76, 453–475.
Carreira-Rosario, A., Bhargava, V., Hillebrand, J., Kollipara, R.K., Ramaswami, M., Buszczak, M., 2016. Repression of Pumilio Protein Expression by Rbfox1 Promotes Germ Cell Differentiation. Developmental Cell 36, 562–571.
Chen, D., McKearin, D., 2003a. Dpp signaling silences bam transcription directly to establish asymmetric divisions of germline stem cells. Current biology : CB 13, 1786–1791.
Chen, D., McKearin, D.M., 2003b. A discrete transcriptional silencer in the bam gene determines asymmetric division of the Drosophila germline stem cell. Development (Cambridge, England) 130, 1159–1170.
Christerson, L.B., McKearin, D.M., 1994. orb Is required for anteroposterior and dorsoventral patterning during Drosophila oogenesis. Genes and Development. https://doi.org/10.1101/gad.8.5.614
Cinalli, R.M., Rangan, P., Lehmann, R., 2008. Germ cells are forever. Cell 132, 559–562.
Cohen, P.E., Pollack, S.E., Pollard, J.W., 2006. Genetic analysis of chromosome pairing, recombination, and cell cycle control during first meiotic prophase in mammals. Endocrine Reviews. https://doi.org/10.1210/er.2005-0017
Collins, K.A., Unruh, J.R., Slaughter, B.D., Yu, Z., Lake, C.M., Nielsen, R.J., Box, K.S., Miller, D.E., Blumenstiel, J.P., Perera, A.G., Malanowski, K.E., Hawley, R.S., 2014a. Corolla Is a Novel Protein That Contributes to the Architecture of the Synaptonemal Complex of Drosophila. Genetics 198, 219–228. https://doi.org/10.1534/genetics.114.165290
Collins, K.A., Unruh, J.R., Slaughter, B.D., Yu, Z., Lake, C.M., Nielsen, R.J., Box, K.S., Miller, D.E., Blumenstiel, J.P., Perera, A.G., Malanowski, K.E., Scott Hawley, R., 2014b. Corolla is a novel protein that contributes to the architecture of the synaptonemal complex of Drosophila. Genetics. https://doi.org/10.1534/genetics.114.165290
Conrad, T., Cavalli, F.M.G., Holz, H., Hallacli, E., Kind, J., Ilik, I., Vaquerizas, J.M., Luscombe, N.M., Akhtar, A., 2012a. The MOF Chromobarrel Domain Controls Genome-wide H4K16 Acetylation and Spreading of the MSL Complex. Developmental Cell. https://doi.org/10.1016/j.devcel.2011.12.016

Conrad, T., Cavalli, F.M.G., Vaquerizas, J.M., Luscombe, N.M., Akhtar, A., 2012b. Drosophila dosage compensation involves enhanced pol II recruitment to male X-linked promoters. Science. https://doi.org/10.1126/science.1221428
De Rooij, D.G., 2017. The nature and dynamics of spermatogonial stem cells. Development (Cambridge). https://doi.org/10.1242/dev.146571
Dong, X., Weng, Z., 2013. The correlation between histone modifications and gene expression. Epigenomics. https://doi.org/10.2217/epi.13.13
Eichhorn, S.W., Subtelny, A.O., Kronja, I., Kwasnieski, J.C., Orr-Weaver, T.L., Bartel, D.P., 2016. mRNA poly(A)-tail changes specified by deadenylation broadly reshape translation in Drosophila oocytes and early embryos. eLife 5, e16955. https://doi.org/10.7554/eLife.16955
Eikenes, Å.H., Malerød, L., Christensen, A.L., Steen, C.B., Mathieu, J., Nezis, I.P., Liestøl, K., Huynh, J.R., Stenmark, H., Haglund, K., 2015. ALIX and ESCRT-III Coordinately Control Cytokinetic Abscission during Germline Stem Cell Division In Vivo. PLoS Genetics. https://doi.org/10.1371/journal.pgen.1004904
El-Brolosy, M.A., Kontarakis, Z., Rossi, A., Kuenne, C., Günther, S., Fukuda, N., Kikhi, K., Boezio, G.L.M., Takacs, C.M., Lai, S.-L., Fukuda, R., Gerri, C., Giraldez, A.J., Stainier, D.Y.R., 2019. Genetic compensation triggered by mutant mRNA degradation. Nature 568, 193–197. https://doi.org/10.1038/s41586-019-1064-z
Eliazer, S., Buszczak, M., 2011. Finding a niche: studies from the Drosophila ovary. Stem cell research & therapy 2, 45. https://doi.org/10.1186/scrt86
Erickson, J.W., 2016. Primary sex determination in Drosophila melanogaster does not rely on the male-specific lethal complex. Genetics. https://doi.org/10.1534/genetics.115.182931
Fayomi, A.P., Orwig, K.E., 2018. Spermatogonial stem cells and spermatogenesis in mice, monkeys and men. Stem Cell Research. https://doi.org/10.1016/j.scr.2018.04.009
Flora, P., McCarthy, A., Upadhyay, M., Rangan, P., 2017. Role of chromatin modifications in Drosophila germline stem cell differentiation, in: Results and Problems in Cell Differentiation. pp. 1–30. https://doi.org/10.1007/978-3-319-44820-6_1
Flora, P., Wong-Deyrup, S.W., Martin, E., Palumbo, R., Nasrallah, M., Oligney, A., Blatt, P., Patel, D., Fuchs, G., Rangan, P., 2018. Sequential regulation of maternal mRNAs through a conserved cis-acting element in their 3 UTRs.
Fuchs, G., Diges, C., Kohlstaedt, L.A., Wehner, K.A., Sarnow, P., 2011. Proteomic analysis of ribosomes: translational control of mRNA populations by glycogen synthase GYS1. Journal of molecular biology 410, 118–130. https://doi.org/10.1016/j.jmb.2011.04.064
Fuller, M.T., Spradling, A.C., 2007. Male and female Drosophila germline stem cells: Two versions of immortality. Science. https://doi.org/10.1126/science.1140861
Gladstein, N., McKeon, M.N., Horabin, J.I., 2010. Requirement of male-specific dosage compensation in Drosophila females-implications of early X chromosome gene expression. PLoS Genetics. https://doi.org/10.1371/journal.pgen.1001041
Gratz, S.J., Cummings, A.M., Nguyen, J.N., Hamm, D.C., Donohue, L.K., Harrison, M.M., Wildonger, J., O\textquoterightConnor-Giles, K.M., 2013. Genome Engineering of Drosophila with the CRISPR RNA-Guided Cas9 Nuclease. Genetics 194, 1029–1035. https://doi.org/10.1534/genetics.113.152710
Gratz, S.J., Rubinstein, C.D., Harrison, M.M., Wildonger, J., O'Connor-Giles, K.M., 2015. CRISPR-Cas9 Genome Editing in Drosophila. Current protocols in molecular biology 111, 31.2.1-31.2.20. https://doi.org/10.1002/0471142727.mb3102s111
Gu, W., Wei, X., Pannuti, A., Lucchesi, J.C., 2000. Targeting the chromatin-remodeling MSL complex of Drosophila to its sites of action on the X chromosome requires both acetyl transferase and ATPase activities. The EMBO journal 19, 5202–5211.
Handel, M.A., Schimenti, J.C., 2010. Genetics of mammalian meiosis: Regulation, dynamics and impact on fertility. Nature Reviews Genetics. https://doi.org/10.1038/nrg2723

Hilfiker, A., Hilfiker-Kleiner, D., Pannuti, A., Lucchesi, J.C., 1997. mof, a putative acetyl transferase gene related to the Tip60 and MOZ human genes and to the SAS genes of yeast, is required for dosage compensation in Drosophila. The EMBO journal 16, 2054–2060.
Hua, B.L., Li, S., Orr-Weaver, T.L., 2014. The role of transcription in the activation of a Drosophila amplification origin. G3 (Bethesda, Md.) 4, 2403–2408. https://doi.org/10.1534/g3.114.014050
Hughes, S.E., Miller, D.E., Miller, A.L., Hawley, R.S., 2018. Female Meiosis: Synapsis, Recombination, and Segregation in Drosophila melanogaster. Genetics 208, 875–908.
Huynh, J.R., St Johnston, D., 2000. The role of BicD, Egl, Orb and the microtubules in the restriction of meiosis to the Drosophila oocyte. Development (Cambridge, England) 127, 2785–2794.
Huynh, J.-R.R., St Johnston, D., 2004. The origin of asymmetry: Early polarisation of the Drosophila germline cyst and oocyte, Current Biology. https://doi.org/10.1016/j.cub.2004.05.040
Kadlec, J., Hallacli, E., Lipp, M., Holz, H., Sanchez-Weatherby, J., Cusack, S., Akhtar, A., 2011. Structural basis for MOF and MSL3 recruitment into the dosage compensation complex by MSL1. Nature structural & molecular biology 18, 142–149.
Kahney, E.W., Snedeker, J.C., Chen, X., 2019. Regulation of Drosophila germline stem cells. Current opinion in cell biology 60, 27–35.
Kai, T., Spradling, A., 2003. An empty Drosophila stem cell niche reactivates the proliferation of ectopic cells. Proceedings of the National Academy of Sciences of the United States of America 100, 4633–4638.
Kelley, R.L., Wang, J., Bell, L., Kuroda, M.I., 1997. Sex lethal controls dosage compensation in Drosophila by a non-splicing mechanism. Nature 387, 195–199.
Keogh, M.-C.C., Kurdistani, S.K., Morris, S.A., Ahn, S.H., Podolny, V., Collins, S.R., Schuldiner, M., Chin, K., Punna, T., Thompson, N.J., Boone, C., Emili, A., Weissman, J.S., Hughes, T.R., Strahl, B.D., Grunstein, M., Greenblatt, J.F., Buratowski, S., Krogan, N.J., 2005. Cotranscriptional set2 methylation of histone H3 lysine 36 recruits a repressive Rpd3 complex. Cell 123, 593–605. https://doi.org/10.1016/j.cell.2005.10.025
Kim, D., Blus, B.J., Chandra, V., Huang, P., Rastinejad, F., Khorasanizadeh, S., 2010. Corecognition of DNA and a methylated histone tail by the MSL3 chromodomain. Nature Structural and Molecular Biology. https://doi.org/10.1038/nsmb.1856
Kim, D., Langmead, B., Salzberg, S.L., 2015. HISAT: a fast spliced aligner with low memory requirements. Nature methods 12, 357–360.
Kimble, J., 2011. Molecular regulation of the mitosis/meiosis decision in multicellular organisms. Cold Spring Harbor perspectives in biology 3, a002683–a002683.
Kirilly, D., Wang, S., Xie, T., 2011. Self-maintained escort cells form a germline stem cell differentiation niche. Development (Cambridge, England) 138, 5087–5097.
Larschan, E., Alekseyenko, A.A., Gortchakov, A.A., Peng, S., Li, B., Yang, P., Workman, J.L., Park, P.J., Kuroda, M.I., 2007. MSL Complex Is Attracted to Genes Marked by H3K36 Trimethylation Using a Sequence-Independent Mechanism. Molecular Cell 28, 121–133. https://doi.org/10.1016/j.molcel.2007.08.011
Lehmann, R., 2012. Germline stem cells: origin and destiny. Cell stem cell 10, 729–739.
Lesch, B.J., Page, D.C., 2012. Genetics of germ cell development. Nature Reviews Genetics. https://doi.org/10.1038/nrg3294
Liao, Y., Smyth, G.K., Shi, W., 2014. featureCounts: an efficient general purpose program for assigning sequence reads to genomic features. Bioinformatics (Oxford, England) 30, 923–930.
Lucchesi, J.C., Kuroda, M.I., 2015. Dosage compensation in Drosophila. Cold Spring Harbor perspectives in biology 7, a019398.

Mach, J.M., Lehmann, R., 1997. An Egalitarian-BicaudalD complex is essential for oocyte specification and axis determination in Drosophila. Genes & development 11, 423–435.
Marston, A.L., Amon, A., 2004. Meiosis: Cell-cycle controls shuffle and deal. Nature Reviews Molecular Cell Biology. https://doi.org/10.1038/nrm1526
Mathieu, J., Huynh, J.R., 2017. Monitoring complete and incomplete abscission in the germ line stem cell lineage of Drosophila ovaries. Methods in Cell Biology. https://doi.org/10.1016/bs.mcb.2016.03.033
Matias, N.R., Mathieu, J., Huynh, J.R., 2015. Abscission Is Regulated by the ESCRT-III Protein Shrub in Drosophila Germline Stem Cells. PLoS Genetics. https://doi.org/10.1371/journal.pgen.1004653
McCarthy, A., Deiulio, A., Martin, E.T., Upadhyay, M., Rangan, P., 2018. Tip60 complex promotes expression of a differentiation factor to regulate germline differentiation in female Drosophila. Molecular Biology of the Cell mbc.E18-06-0385. https://doi.org/10.1091/mbc.E18-06-038
McKearin, D., Ohlstein, B., 1995. A role for the Drosophila bag-of-marbles protein in the differentiation of cystoblasts from germline stem cells. Development (Cambridge, England) 121, 2937–2947.
McKearin, D.M., Spradling, A.C., 1990. bag-of-marbles: a Drosophila gene required to initiate both male and female gametogenesis. Genes & development 4, 2242–2251.
Meller, V.H., Wu, K.H., Roman, G., Kuroda, M.I., Davis, R.L., 1997. roX1 RNA paints the X chromosome of male Drosophila and is regulated by the dosage compensation system. Cell 88, 445–457.
Morris, L.X., Spradling, A.C., 2011. Long-term live imaging provides new insight into stem cell regulation and germline-soma coordination in the Drosophila ovary. Development (Cambridge, England) 138, 2207–2215.
Morrison, S.J., Spradling, A.C., 2008. Stem cells and niches: mechanisms that promote stem cell maintenance throughout life. Cell 132, 598–611.
Moschall, R., Strauss, D., García-Beyaert, M., Gebauer, F., Medenbach, J., 2018. Drosophila sister-of-sex-lethal is a repressor of translation. RNA. https://doi.org/10.1261/rna.063776.117
Mukai, M., Hira, S., Nakamura, K., Nakamura, S., Kimura, H., Sato, M., Kobayashi, S., 2015. H3K36 Trimethylation-Mediated Epigenetic Regulation is Activated by Bam and Promotes Germ Cell Differentiation During Early Oogenesis in Drosophila. Biology open 4, 119–124.
Nakayama, J., Rice, J.C., Strahl, B.D., Allis, C.D., Grewal, S.I.S., 2001. Role of Histone H3 Lysine 9 Methylation in Epigenetic Control of Heterochromatin Assembly. Science 292, 110 LP – 113. https://doi.org/10.1126/science.1060118
Navarro, C., Lehmann, R., Morris, J., 2001. Oogenesis: Setting one sister above the rest. Current biology : CB 11, R162-5. https://doi.org/10.1016/S0960-9822(01)00083-5
Navarro-Costa, P., McCarthy, A., Prudêncio, P., Greer, C., Guilgur, L.G., Becker, J.D., Secombe, J., Rangan, P., Martinho, R.G., 2016. Early programming of the oocyte epigenome temporally controls late prophase i transcription and chromatin remodelling. Nature Communications 7. https://doi.org/10.1038/ncomms12331
Ohlstein, B., McKearin, D., 1997. Ectopic expression of the Drosophila Bam protein eliminates oogenic germline stem cells. Development (Cambridge, England) 124, 3651–3662.
Page, S.L., Hawley, R.S., 2001. c(3)G encodes a Drosophila synaptonemal complex protein. Genes & development 15, 3130–3143.
Parisi, M., Nuttall, R., Edwards, P., Minor, J., Naiman, D., Lü, J., Doctolero, M., Vainer, M., Chan, C., Malley, J., Eastman, S., Oliver, B., 2004. A survey of ovary-, testis-, and soma-biased gene expression in Drosophila melanogaster adults. Genome biology 5, R40–R40. https://doi.org/10.1186/gb-2004-5-6-r40

Parisi, M.J., Deng, W., Wang, Z., Lin, H., 2001. The arrest gene is required for germline cyst formation during Drosophila oogenesis. Genesis (New York, N.Y. : 2000) 29, 196–209.
Samata, M., Akhtar, A., 2018. Dosage Compensation of the X Chromosome: A Complex Epigenetic Assignment Involving Chromatin Regulators and Long Noncoding RNAs. Annual Review of Biochemistry. https://doi.org/10.1146/annurev-biochem-062917-011816
Sanchez, C.G., Teixeira, F.K., Czech, B., Preall, J.B., Zamparini, A.L., Seifert, J.R.K., Malone, C.D., Hannon, G.J., Lehmann, R., 2016. Regulation of Ribosome Biogenesis and Protein Synthesis Controls Germline Stem Cell Differentiation. Cell stem cell 18, 276–290.
Shalaby, N.A., Sayed, R., Zhang, Q., Scoggin, S., Eliazer, S., Rothenfluh, A., Buszczak, M., 2017. Systematic discovery of genetic modulation by Jumonji histone demethylases in Drosophila. Scientific Reports. https://doi.org/10.1038/s41598-017-05004-w
Soh, Y.Q.S., Junker, J.P., Gill, M.E., Mueller, J.L., van Oudenaarden, A., Page, D.C., 2015. A Gene Regulatory Program for Meiotic Prophase in the Fetal Ovary. PLoS Genetics. https://doi.org/10.1371/journal.pgen.1005531
Spedale, G., Timmers, H.T.M., Pijnappel, W.W.M.P., 2012. ATAC-king the complexity of SAGA during evolution. Genes & development 26, 527–541.
Spradling, A., Drummond-Barbosa, D., Kai, T., 2001. Stem cells find their niche. Nature 414, 98–104.
Spradling, A., Fuller, M.T., Braun, R.E., Yoshida, S., 2011. Germline stem cells. Cold Spring Harbor Perspectives in Biology 3, a002642–a002642. https://doi.org/10.1101/cshperspect.a002642
Spradling, A.C., de Cuevas, M., Drummond-Barbosa, D., Keyes, L., Lilly, M., Pepling, M., Xie, T., 1997. The Drosophila germarium: stem cells, germ line cysts, and oocytes. Cold Spring Harbor symposia on quantitative biology 62, 25–34.
Spradling, A.C., Nystul, T., Lighthouse, D., Morris, L., Fox, D., Cox, R., Tootle, T., Frederick, R., Skora, A., 2008. Stem cells and their niches: integrated units that maintain Drosophila tissues. Cold Spring Harbor symposia on quantitative biology 73, 49–57.
Stabell, M., Larsson, J., Aalen, R.B., Lambertsson, A., 2007. Drosophila dSet2 functions in H3-K36 methylation and is required for development. Biochemical and Biophysical Research Communications 359, 784–789.
Strukov, Y.G., Sural, T.H., Kuroda, M.I., Sedat, J.W., 2011. Evidence of activity-specific, radial organization of mitotic chromosomes in Drosophila. PLoS biology 9, e1000574.
Suganuma, T., Gutiérrez, J.L., Li, B., Florens, L., Swanson, S.K., Washburn, M.P., Abmayr, S.M., Workman, J.L., 2008. ATAC is a double histone acetyltransferase complex that stimulates nucleosome sliding. Nature structural & molecular biology 15, 364–372.
Sugimura, I., Lilly, M.A., 2006. Bruno inhibits the expression of mitotic cyclins during the prophase I meiotic arrest of Drosophila oocytes. Developmental Cell 10, 127–135.
Sun, J., Wei, H.-M., Xu, J., Chang, J.-F., Yang, Z., Ren, X., Lv, W.-W., Liu, L.-P., Pan, L.-X., Wang, X., Qiao, H.-H., Zhu, B., Ji, J.-Y., Yan, D., Xie, T., Sun, F.-L., Ni, J.-Q., 2015. Histone H1-mediated epigenetic regulation controls germline stem cell self-renewal by modulating H4K16 acetylation. Nature communications 6, 8856. https://doi.org/10.1038/ncomms9856
Sural, T.H., Peng, S., Li, B., Workman, J.L., Park, P.J., Kuroda, M.I., 2008. The MSL3 chromodomain directs a key targeting step for dosage compensation of the Drosophila melanogaster X chromosome. Nature structural & molecular biology 15, 1318–1325.
Tastan, O.Y., Maines, J.Z., Li, Y., McKearin, D.M., Buszczak, M., 2010. Drosophila ataxin 2-binding protein 1 marks an intermediate step in the molecular differentiation of female germline cysts. Development (Cambridge, England) 137, 3167–3176.

THE MODENCODE CONSORTIUM, Roy, S., Ernst, J., Kharchenko, P.V., Kheradpour, P., Negre, N., Eaton, M.L., Landolin, J.M., Bristow, C.A., Ma, L., Lin, M.F., Washietl, S., Arshinoff, B.I., Ay, F., Meyer, P.E., Robine, N., Washington, N.L., Di Stefano, L., Berezikov, E., Brown, C.D., Candeias, R., Carlson, J.W., Carr, A., Jungreis, I., Marbach, D., Sealfon, R., Tolstorukov, M.Y., Will, S., Alekseyenko, A.A., Artieri, C., Booth, B.W., Brooks, A.N., Dai, Q., Davis, C.A., Duff, M.O., Feng, X., Gorchakov, A.A., Gu, T., Henikoff, J.G., Kapranov, P., Li, R., MacAlpine, H.K., Malone, J., Minoda, A., Nordman, J., Okamura, K., Perry, M., Powell, S.K., Riddle, N.C., Sakai, A., Samsonova, A., Sandler, J.E., Schwartz, Y.B., Sher, N., Spokony, R., Sturgill, D., van Baren, M., Wan, K.H., Yang, L., Yu, C., Feingold, E., Good, P., Guyer, M., Lowdon, R., Ahmad, K., Andrews, J., Berger, B., Brenner, S.E., Brent, M.R., Cherbas, L., Elgin, S.C.R., Gingeras, T.R., Grossman, R., Hoskins, R.A., Kaufman, T.C., Kent, W., Kuroda, M.I., Orr-Weaver, T., Perrimon, N., Pirrotta, V., Posakony, J.W., Ren, B., Russell, S., Cherbas, P., Graveley, B.R., Lewis, S., Micklem, G., Oliver, B., Park, P.J., Celniker, S.E., Henikoff, S., Karpen, G.H., Lai, E.C., MacAlpine, D.M., Stein, L.D., White, K.P., Kellis, M., Acevedo, D., Auburn, R., Barber, G., Bellen, H.J., Bishop, E.P., Bryson, T.D., Chateigner, A., Chen, J., Clawson, H., Comstock, C.L.G., Contrino, S., DeNapoli, L.C., Ding, Q., Dobin, A., Domanus, M.H., Drenkow, J., Dudoit, S., Dumais, J., Eng, T., Fagegaltier, D., Gadel, S.E., Ghosh, S., Guillier, F., Hanley, D., Hannon, G.J., Hansen, K.D., Heinz, E., Hinrichs, A.S., Hirst, M., Jha, S., Jiang, L., Jung, Y.L., Kashevsky, H., Kennedy, C.D., Kephart, E.T., Langton, L., Lee, O.-K., Li, S., Li, Z., Lin, W., Linder-Basso, D., Lloyd, P., Lyne, R., Marchetti, S.E., Marra, M., Mattiuzzo, N.R., McKay, S., Meyer, F., Miller, D., Miller, S.W., Moore, R.A., Morrison, C.A., Prinz, J.A., Rooks, M., Moore, R., Rutherford, K.M., Ruzanov, P., Scheftner, D.A., Senderowicz, L., Shah, P.K., Shanower, G., Smith, R., Stinson, E.O., Suchy, S., Tenney, A.E., Tian, F., Venken, K.J.T., Wang, H., White, R., Wilkening, J., Willingham, A.T., Zaleski, C., Zha, Z., Zhang, D., Zhao, Y., Zieba, J., 2010. Identification of Functional Elements and Regulatory Circuits by Drosophila modENCODE. Science 330, 1787–1797. https://doi.org/10.1126/science.1198374

Theurkauf, W.E., Alberts, B.M., Jan, Y.N., Jongens, T.A., 1993. A central role for microtubules in the differentiation of Drosophila oocytes. Development (Cambridge, England) 118, 1169–1180.

Turner, B.M., Birley, A.J., Lavender, J., 1992. Histone H4 isoforms acetylated at specific lysine residues define individual chromosomes and chromatin domains in Drosophila polytene nuclei. Cell 69, 375–384.

UCHIDA, S., UENOYAMA, T., OISHI, K., 1981. Studies on the sex-specific lethals of Drosophila melanogaster. III. A third chromosome male-specific lethal mutant. The Japanese journal of genetics 56, 523–527.

Upadhyay, M., Kuna, M., Tudor, S., Martino Cortez, Y., Rangan, P., 2018. A switch in the mode of Wnt signaling orchestrates the formation of germline stem cell differentiation niche in Drosophila. PLoS genetics 14, e1007154.

Upadhyay, M., Martino Cortez, Y., Wong-Deyrup, S., Tavares, L., Schowalter, S., Flora, P., Hill, C., Nasrallah, M.A., Chittur, S., Rangan, P., 2016. Transposon Dysregulation Modulates dWnt4 Signaling to Control Germline Stem Cell Differentiation in Drosophila. PLoS genetics 12, e1005918.

Von Stetina, J.R., Orr-Weaver, T.L., 2011. Developmental control of oocyte maturation and egg activation in metazoan models. Cold Spring Harbor Perspectives in Biology 3, a005553. https://doi.org/10.1101/cshperspect.a005553

Wang, Z., Lin, H., 2007. Sex-lethal is a target of Bruno-mediated translational repression in promoting the differentiation of stem cell progeny during Drosophila oogenesis. Developmental biology 302, 160–168.

Xie, T., 2013. Control of germline stem cell self-renewal and differentiation in the Drosophila ovary: concerted actions of niche signals and intrinsic factors. Wiley interdisciplinary reviews. Developmental biology 2, 261–273.
Xie, T., 2000. A Niche Maintaining Germ Line Stem Cells in the Drosophila Ovary. Science (New York, N.Y.) 290, 328–330.
Xie, T., Spradling, A.C., 2000. A niche maintaining germ line stem cells in the Drosophila ovary. Science 290, 328–330. https://doi.org/10.1126/science.290.5490.328
Xie, T., Spradling, A.C., 1998. decapentaplegic is essential for the maintenance and division of germline stem cells in the Drosophila ovary. Cell 94, 251–260.
Yap, K.L., Zhou, M.-M., 2011. Structure and mechanisms of lysine methylation recognition by the chromodomain in gene transcription. Biochemistry 50, 1966–1980. https://doi.org/10.1021/bi101885m
Zhang, Q., Shalaby, N.A., Buszczak, M., 2014. Changes in rRNA transcription influence proliferation and cell fate within a stem cell lineage. Science (New York, N.Y.) 343, 298–301. https://doi.org/10.1126/science.1246384

Figures:

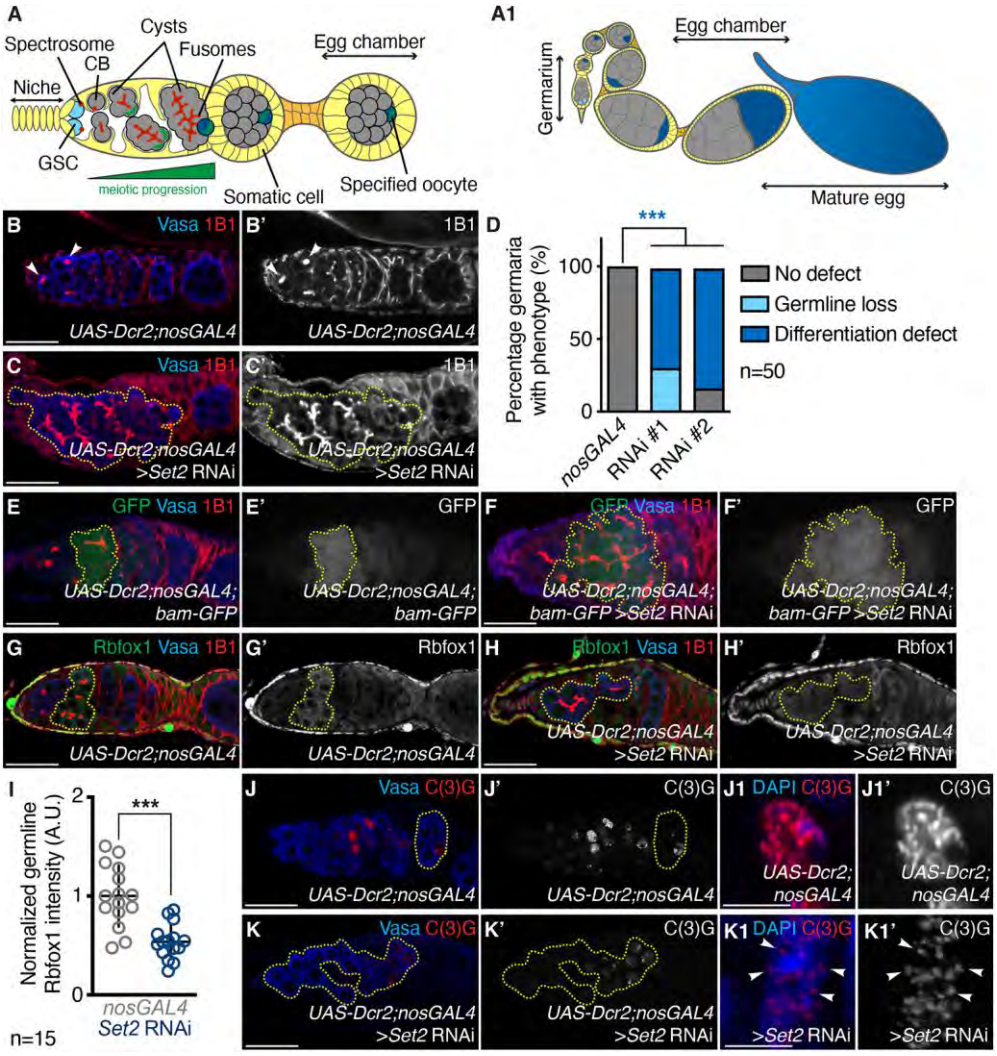

Figure 1. Set2 is required in the germline for differentiaiton during oogenesis
(A) A schematic of a *Drosophila* germarium where germ cells (gray, light and dark blue) are surrounded by somatic cells (yellow). Germ cells differentiate and specify an oocyte (green/blue).

(A1) A schematic of a *Drosophila* ovariole showing egg chambers that house a maturing oocyte (blue) connected by somatic cells (orange).

(B-B') Control and (C-C') germline depleted *Set2* (RNAi line #1) germaria stained for Vasa (blue) and 1B1 (red) shows that *Set2* germline depletion results in differentiation defects such as accumulation of irregular cysts with >16 cells (yellow dashed outline), accumulation of 16-cell cysts close to the niche and loss of GSCs (white arrows in

control). 1B1 channel is shown in B' and C'. Quantitation in (D), Fisher's exact test; *** indicates *p<0.001*.

(E-E') Control and (F-F') germline depleted *Set2* germaria both carrying a *bam-GFP* transgene stained for GFP (green), Vasa (blue), and 1B1 (red) shows that *Set2* germline depletion results in irregular GFP-positive cysts compared to control (yellow dashed outline) (90% in *Set2* RNAi compared to 4% in *nosGAL4*; *p<2.2E-16*, n=50, Fisher's exact test). GFP channel is shown in E' and F'.

(G-G') Control and (H-H') germline depleted *Set2* germaria stained for Rbfox1 (green), Vasa (blue), and 1B1 (red) shows that *Set2* germline depletion results in decreased levels of Rbfox1 in the germline compared to control (yellow dashed outline). Rbfox1 channel is shown in G' and H'. Quantitation in (I), Student t-test; ** indicates *p<0.01*; *** indicates *p<0.001*.

(J-J' and J1-J1') Control and (K-K' and K1-K1') germline depleted *Set2* germaria stained for Vasa (blue) and C(3)G (red) shows that *Set2* germline depletion results in aberrant C(3)G staining compared to control (yellow dashed outline) (100% in *Set2* RNAi compared to 2% in *nosGAL4*; *p<2.2E-16*, n=50) and improper assembly of the synaptonemal complex (white arrows). Statistical analysis, Fisher's exact test. C(3)G channel is shown in J', J1', K1, and K1'.

Scale bar for J1-J1' and K1-K1' is 2 μm, scale bar for all other images is 20 μm.

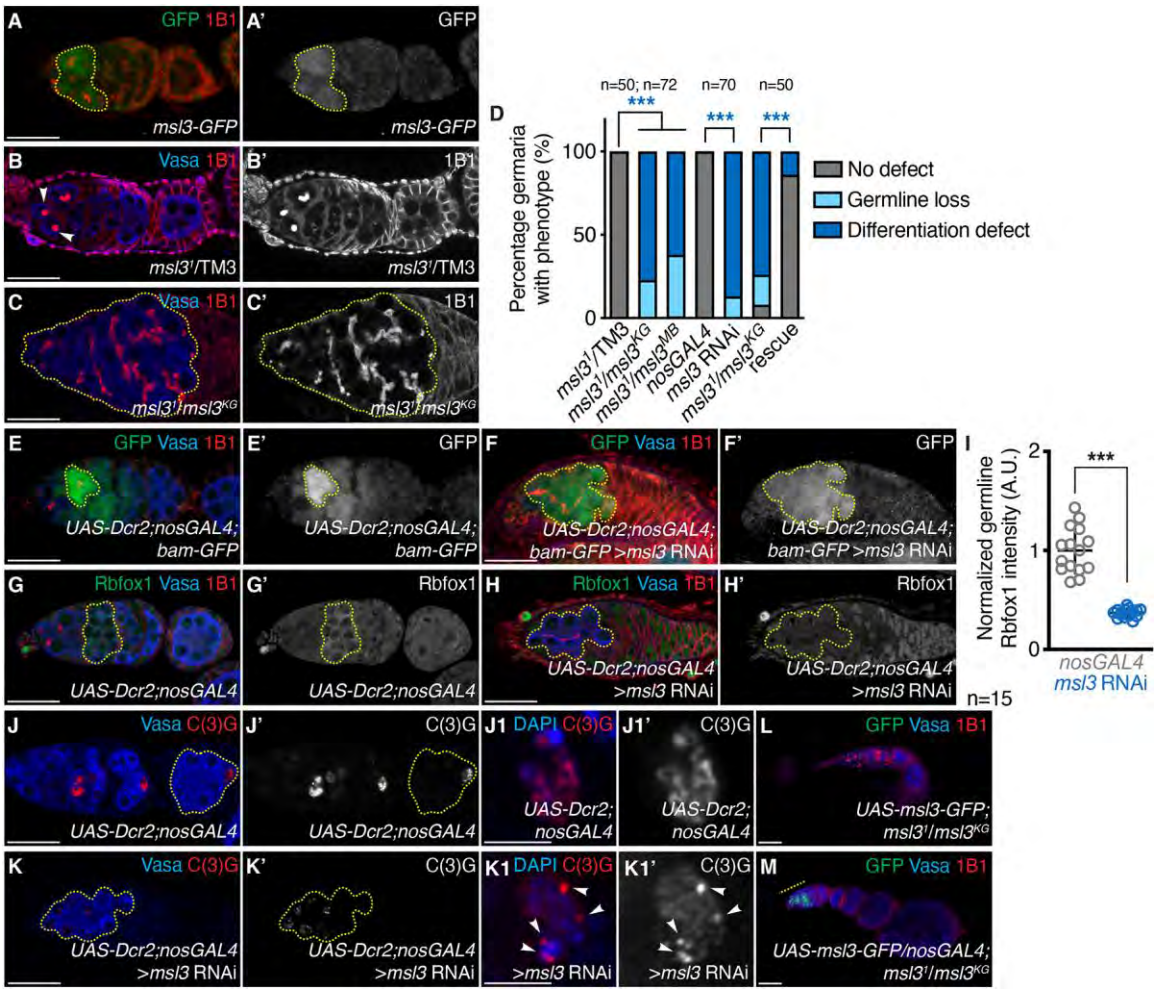

Figure 2. MSL3 is required in the germline for differentiation

(A-A') *msl3-GFP* germarium stained for GFP (green) and 1B1 (red). GFP expression is enriched in single cells and early cysts, showing that MSL3 is expressed in the mitotic and early meiotic stages of oogenesis. GFP channel is shown in A'.

(B-B') Heterozygous control and (C-C') trans-allelic *msl3* mutant germaria stained for Vasa (blue) and 1B1 (red) shows that *msl3* mutants have differentiation defects such as accumulation of irregular cysts with >16 cells (yellow dashed outline), accumulation of 16-cell cysts close to the niche and and loss of GSCs. 1B1 channel is shown in B' and C'. Quantitation in (D), Fisher's exact test; *** indicates $p<0.001$).

(E-E') Control and (F-F') germline depleted *msl3* germaria both carrying a *bam-GFP* transgene stained for GFP (green), Vasa (blue), and 1B1 (red) shows that *msl3* germline depletion results in irregular GFP-positive cysts compared to control (yellow dashed outline) (96% in *msl3* RNAi compared to 0% in *nosGAL4*; $p<2.2E-16$, n=50, Fisher's exact test). GFP channel is shown in E' and F'.

(G-G') Control and (H-H') germline depleted *msl3* germaria stained for Rbfox1 (green), Vasa (blue), and 1B1 (red) shows that *msl3* germline depletion results in decreased levels of Rbfox1 in the germline compared to control (yellow dashed outline). Rbfox1 channel is shown in G' and H'. Quantitation in (I), Student t-test; ** indicates *p<0.01*.

(J-J') Control and (K-K') germline depleted *msl3* germaria stained for Vasa (blue) and C(3)G (red) shows that *msl3* germline depletion results in aberrant C(3)G staining compared to control (yellow dashed outline) (100% in *msl3* RNAi compared to 0% in *nosGAL4*; *p<2.2E-16*, n=50, Fisher's exact test) and improper assembly of the synaptonemal complex (white arrows). C(3)G channel is shown in J', J1', K1, and K1'.

(L) Control and (M) germline overexpression of *msl3* in *msl3* mutant germaria stained for GFP (green), Vasa (blue), and 1B1 (red) shows that *msl3* germline overexpression in *msl3* mutants results in reduced frequency of irregular cysts (yellow dashed line) (14% in *msl3* rescue compared to 74% in *msl3* mutant; *p<2.2E-16*, n=50) and germline loss (0% in *msl3* rescue compared to 18% in *msl3* mutant; *p=0.0002*, n=50). Quantitation in (D); Fisher's exact test.

Scale bar for J1-J1' and K1-K1' is 2 μm, scale bar for all other images is 20 μm.

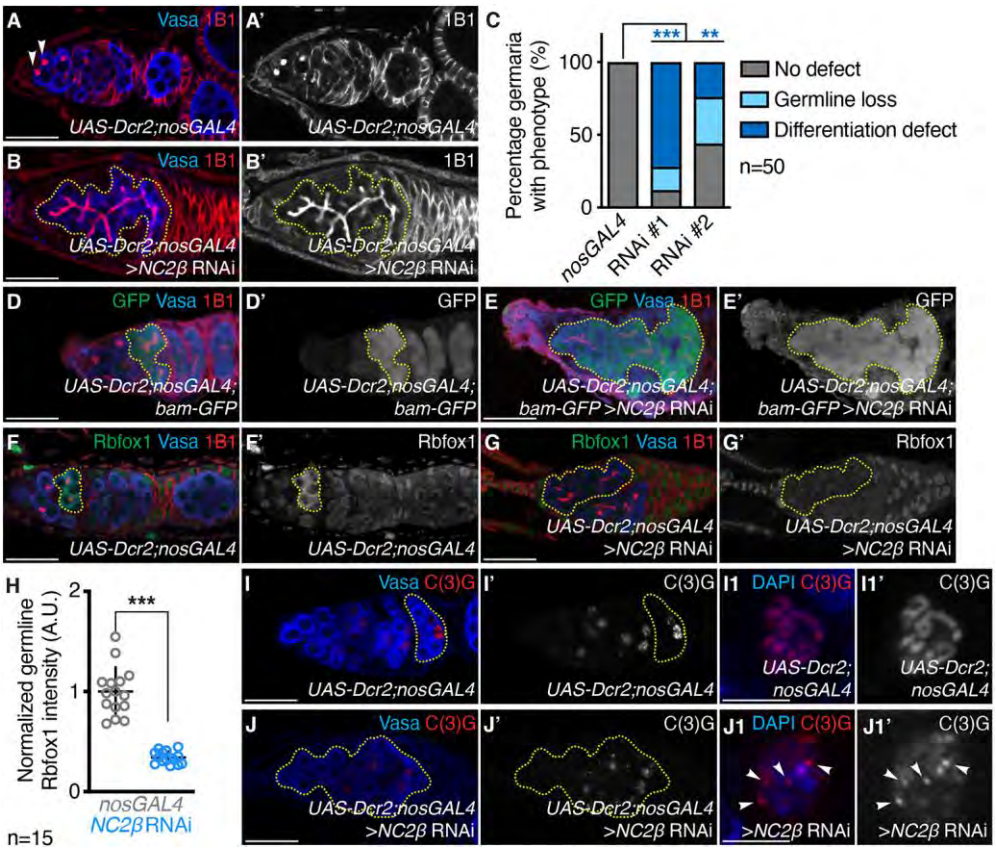

Figure 3. ATAC component, NC2β, is required in the germline for differentiation
(A-A') Control and (B-B') germline depleted *NC2β* germaria stained for Vasa (blue) and 1B1 (red) shows that *NC2β* germline depletion results in differentiation defects such as accumulation of irregular cysts with >16 cells (yellow dashed outline), accumulation of 16-cell cysts close to the niche and loss of GSCs. 1B1 channel is shown in A' and B'. Quantitation in (C), Fisher's exact; ** indicates *p<0.01* and *** indicates *p<0.001*.

(D-D') Control and (E-E') germline depleted *NC2β* germaria both carrying a *bam-GFP* transgene stained for GFP (green), Vasa (blue), and 1B1 (red) shows that *NC2β* germline depletion results in accumulation of irregular GFP-positive cysts compared to control (yellow dashed outline) (64% in *NC2β* RNAi compared to 0% in *nosGAL4*; *p=2.5E-13*, n=50, Fisher's exact test). GFP channel is shown in D' and E'.

(F-F') Control and (G-G') germline depleted *NC2β* germaria stained for Rbfox1 (green), Vasa (blue), and 1B1 (red) shows that *NC2β* germline depletion results in decreased levels of Rbfox1 in the germline compared to control (yellow dashed outline). Rbfox1 channel is shown in F' and G'. Quantitation in (H), Student t-test; *** indicates *p<0.001*.

(I-I’ and I1-I1’) Control and (J-J’ and J1-J1’) germline depleted *NC2β* germaria stained for Vasa (blue) and C(3)G (red) shows that *NC2β* germline depletion results in aberrant C(3)G staining compared to control (yellow dashed outline and white arrows) (75% in *NC2β* RNAi compared to 0% in *nosGAL4*; $p<2.2E-16$, n=50) and improper assembly of the synaptonemal complex (white arrows). Statistical analysis, Fisher’s exact test. C(3)G channel is shown in I’, I1’, J’, and J1’.

Scale bar for I1-I1’ and J1-J1’ is 2μm, scale bar for all other images is 20μm.

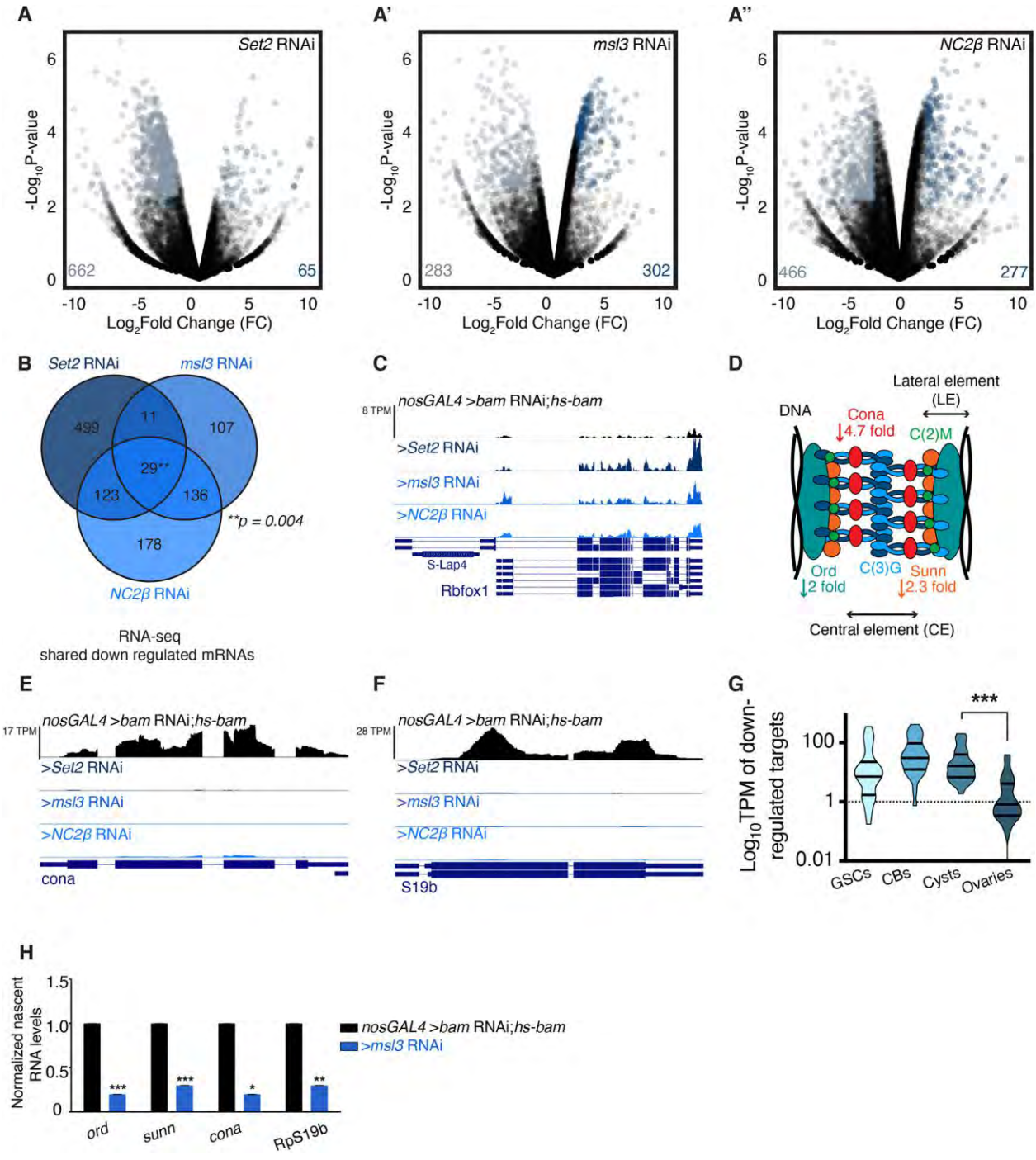

Figure 4. Set2, MSL3, and ATAC complex regulate mRNA levels of recombination machinery components, but not *Rbfox1*

(A-A'') Volcano plots of $-Log_{10}$P-value vs. Log_2Fold Change (FC) of (A) *Set2*, (A') *msl3*, and (A'') *NC2β* germline depleted ovaries compared to *bam* RNAi;*hs-bam*. (Genes with four-fold or higher change were considered significant (FDR = 0.05).

(B) Venn diagram of downregulated genes from RNA-seq of *Set2*, *msl3*, and *NC2β* germline depleted ovaries compared to *bam* RNAi;*hs-bam*.

(C) RNA-seq track showing that *Rbfox1* is not reduced upon germline depletion of *Set2*, *msl3*, and *NC2β*.

(D) A structural model of the SC consisting of proteins such as Ord (teal), Sunn (orange), and C(2)M (green) assemble along DNA. Down arrows denote fold downregulation of SC components in depleted ovaries.

(E) RNA-seq track showing that *cona* is reduced upon germline depletion of *Set2*, *msl3*, and *NC2β*.

(F) RNA-seq track showing that *RpS19b* is reduced upon germline depletion of *Set2*, *msl3*, and *NC2β*.

(G) Violin plot of mRNA levels of the 29 shared downregulated targets in ovaries enriched for GSCs, GSC daughters, cysts, and whole ovaries, showing that the shared targets are expressed upto cyst stages, that then attenuated in whole ovaries (one-way ANOVA; *** indicates $p<0.001$)

(H) qRT-PCR measuring levels of nascent mRNA levels of *ord*, *sunn*, *cona* and *RpS19b* upon depletion of *msl3* showing reduction compared to developmental control.

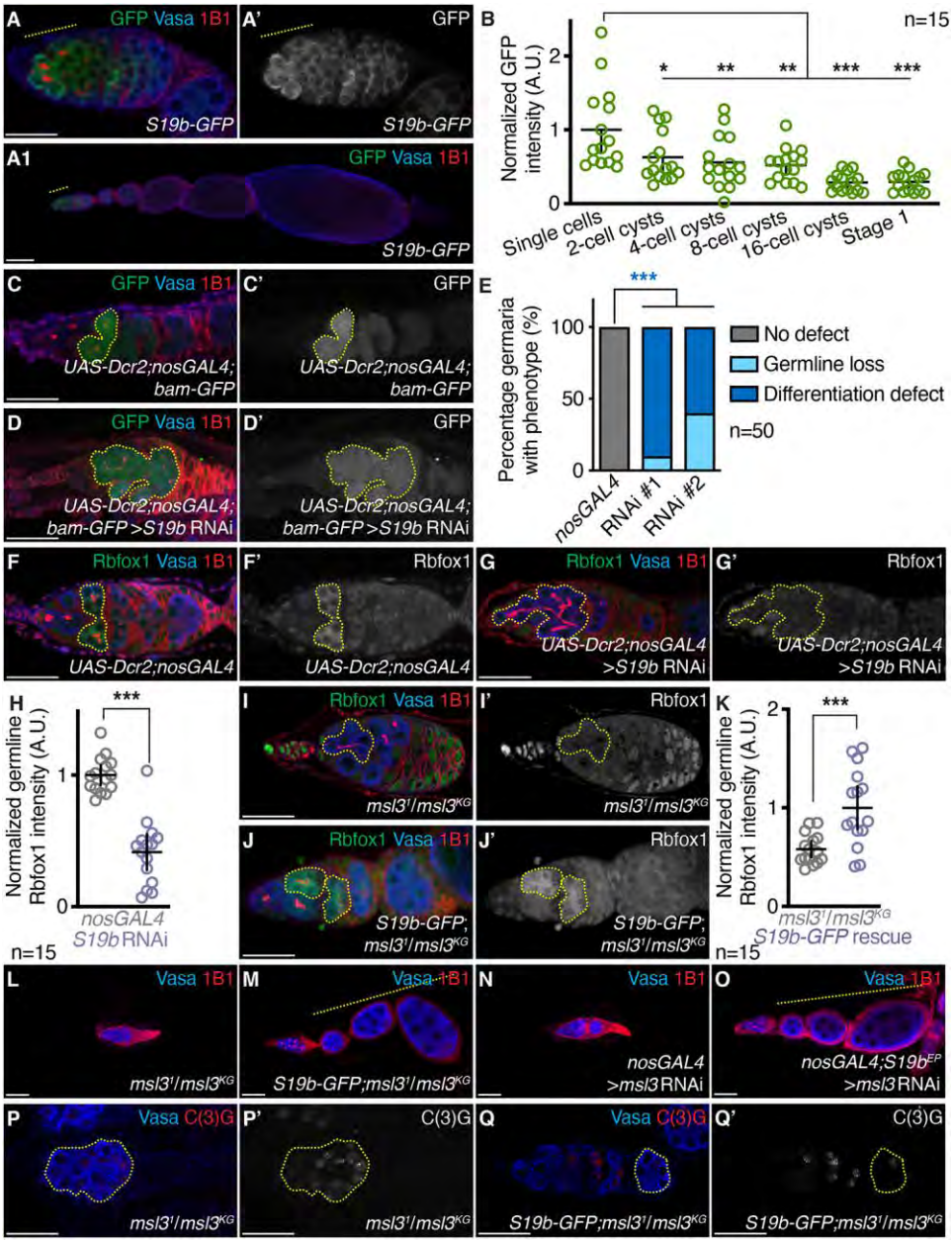

Figure 5. RpS19b, a germline-enriched paralog, is expressed in the mitotic and early meiotic stages and is required for Rbfox1 expression

(A-A') *RpS19b-GFP* germarium and (A1) ovariole stained for GFP (green), Vasa (blue), and 1B1 (red). GFP is upto the cyst stages and then attenuated. GFP channel is shown in A'. Quantitation in (B), one-way ANOVA; * indicates *p<0.05*, ** indicates *p<0.01*, and *** indicates *p<0.001*.

(C-C') Control and (D-D') germline depleted *RpS19b* germaria both carrying a *bam-GFP* transgene stained for GFP (green), Vasa (blue), and 1B1 (red) shows cysts with >16 cell that are GFP-positive in *RpS19b* germline depletion compared to control (yellow

dashed outline). GFP channel is shown in C' and D'. Quantitation in (E), Fisher's exact test on differentiation defect; *** indicates *p<0.001*.

(F-F') Control and (G-G') germline depleted *RpS19b* germaria stained for Rbfox1 (green), Vasa (blue), and 1B1 (red) shows that *RpS19b* germline depletion results in decreased levels of Rbfox1 compared to control (yellow dashed outline). Rbfox1 channel is shown in F' and G'. Quantitation in (H), Student t-test; *** indicates *p<0.001*.

(I-I') Control and (J-J') *RpS19b-GFP* rescue germaria stained for Rbfox1 (green), Vasa (blue), and 1B1 (red) shows that addition of *RpS19b-GFP* to *msl3* mutants results in increased levels of Rbfox1 expression compared to control. Rbfox1 channel is shown in I' and J'. Quantitation in (K), Student t-test; *** indicates *p<0.001*.

(L) Control and (M) *RpS19b-GFP* rescue ovarioles stained for Vasa (blue) and 1B1 (red) shows that addition of *RpS19b-GFP* to *msl3* mutants results in an increased frequency of spectrosomes and cysts (92% in *RpS19b-GFP* rescue compared to 4% in $msl3^{1}/msl3^{KG}$; *p<2.2E-16*, n=50) and subsequent egg chambers compared to control (yellow dashed outline) (98% in *RpS19b-GFP* rescue compared to 16% in $msl3^{1}/msl3^{KG}$; *p<2.2E-16*, n=50, Fisher's exact test).

(N) Control and (O) $RpS19b^{EP}$ rescue ovarioles stained for Vasa (blue) and 1B1 (red) shows that expression of $RpS19b^{EP}$ in *msl3* germline depletion ovaries results in an increased frequency of spectrosomes and cysts (90% in $RpS19b^{EP}$ rescue compared to 0% in *msl3* RNAi; *p<2.2E-16*, n=50) and subsequent egg chambers compared to control (yellow dashed outline) (100% in $RpS19b^{EP}$ rescue compared to 4% in *msl3* RNAi; *p<2.2E-16*, n=50, Fisher's exact test).

(P-P') Control and (Q-Q') *RpS19b-GFP* rescue germaria stained for Vasa (blue) and C(3)G (red) shows that rescue and control germaria have aberrant C(3)G expression (yellow dashed outline) (96% in *RpS19b-GFP* rescue compared to 100% in $msl3^{1}/msl3^{KG}$; *p=0.5*, n=50). Addition of *RpS19b-GFP* does not rescue egg laying defects (38 eggs/female in *RpS19b-GFP*, 32 eggs/female in $msl3^{1}$ heterozygote, 101 eggs/female in $msl3^{KG}$ heterozygote compared to 0 eggs/female in $msl3^{KG}/msl3^{1}$ and rescue; *p=0.02* for $msl3^{KG}/msl3^{1}$ and *p=0.03* for rescue, n=4, Fisher's exact test). C(3)G channel is shown in P' and Q'.

Scale bar for all images is 20 μm.

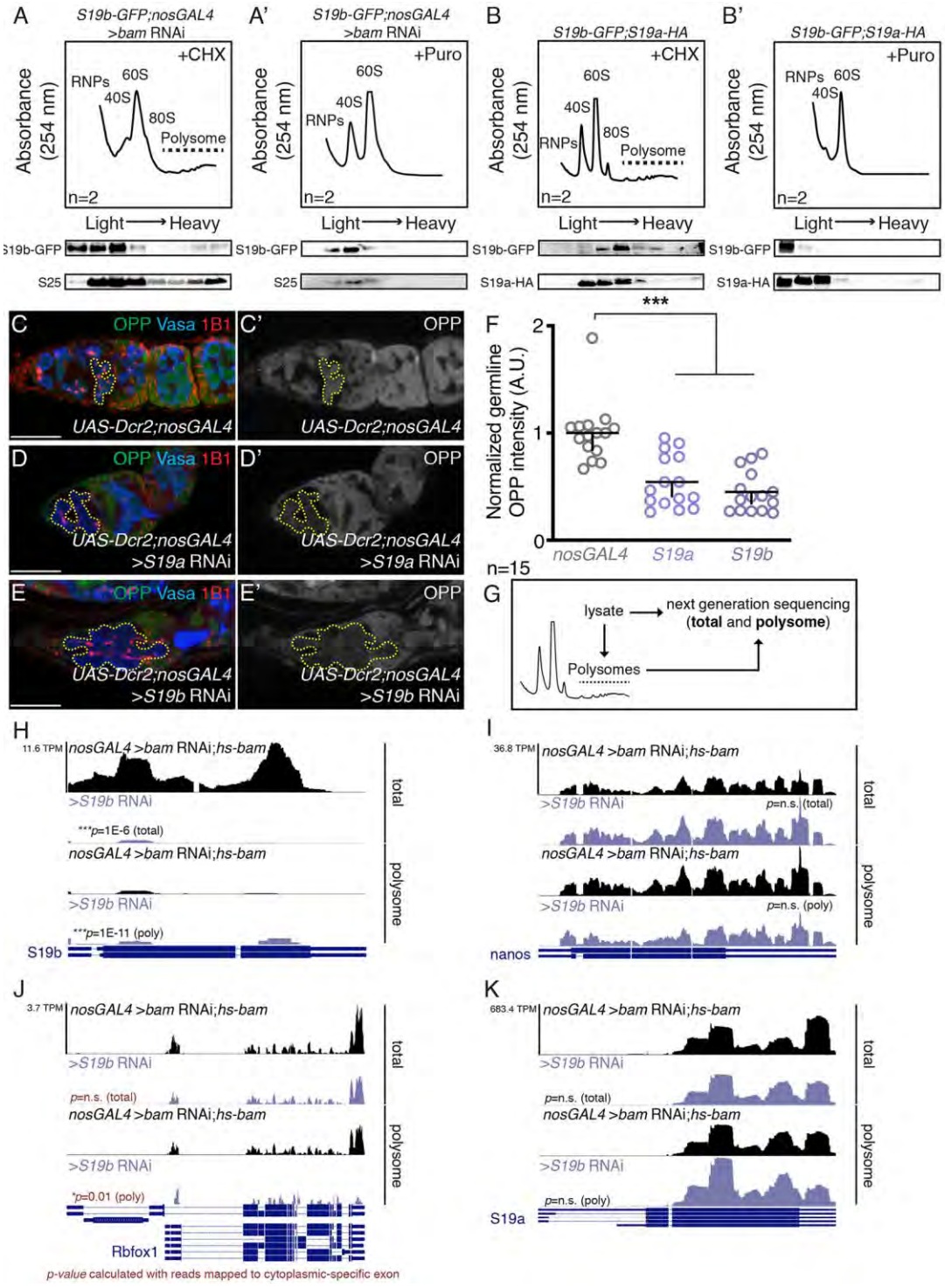

Figure 6. RpS19 paralogs are incorporated into the ribosome and RpS19 levels affect translation, including translation of Rbfox1

(A) Top: Polysome profiles of *RpS19b-GFP;nosGAL4 >bam* RNAi ovaries treated with cycloheximide (CHX) or (A') puromycin. Bottom: Western blot of A) cycloheximide (CHX) or (A') puromycin. Blots were stained for GFP (top) and RpS25 (bottom),

showing RpS19b and RpS25 bands in heavy fractions in CHX-treated samples that are absent in puromycin treated samples.

(B) Top: Polysome profiles of *RpS19b-GFP;RpS19a-HA* whole ovaries treated with cycloheximide (CHX) or (B') puromycin. Bottom: Western blot of (B) cycloheximide (CHX) or (B') puromycin. Blots were stained for HA (top) and GFP (bottom), showing RpS19a and RpS19b bands in heavy fractions in CHX-treated samples that are absent in puromycin treated samples.

(C-C') Control, (D-D') germline depleted *RpS19a* and (E-E') *RpS19b* germaria pulsed with OPP (green) and stained for Vasa (blue) and 1B1 (red) shows that *RpS19a* and *RpS19b* germline depletion results in decreased OPP compared to control. OPP channel is shown in C', D', and E'. Quantitation in (F), one-way ANOVA; *** indicates $p<0.001$.

(G) A schematic of the experimental approach to polysome-seq: RNA is extracted (total) with polysome fractionation (polysome) followed by sequencing.

(H) RNA-seq track of total (top) and polysome (bottom) showing that *RpS19b* is reduced upon germline depletion of *RpS19b* (purple) compared to control (black) (total: $Log_2FC=-4.1$, $p=1E-6$, n=2 and polysome: $Log_2FC=-4.5$; $p=1E-11$, n=2). Statistical analysis, Student t-test; *** indicates $p<0.001$.

(I) RNA-seq track of total (top) and polysome (bottom) showing that *nanos* and amount of germline is not reduced upon germline depletion of *RpS19b* (purple) compared to control (black) (total: $Log_2FC=0.4$; $p=0.4$, n=2 and polysome: $Log_2FC=0.3$; $p=0.7$, n=2). Statistical analysis, Student t-test; "n.s." indicates $p>0.5$.

(J) RNA-seq track of total (top) and polysome (bottom) showing that cytoplasmic *Rbfox1* is reduced in polysome fractions upon germline depletion of *RpS19b* (purple) compared to control (black) (total: $p=0.2$, n=2 and polysome: $p=0.01$, n=2). Statistical analysis, Student t-test; "n.s." indicates $p>0.5$ and * indicates $p<0.05$.

(K) RNA-seq track of total (top) and polysome (bottom) showing that *RpS19a* is not reduced upon germline depletion of *RpS19b* (purple) compared to control (black) (total: $Log_2FC=-0.4$; $p=0.4$, n=2 and polysome: $Log_2FC=-0.1$; $p=0.9$, n=2). Statistical analysis, Student t-test; "n.s." indicates $p>0.5$.

Scale bar for all images is 20 μm.

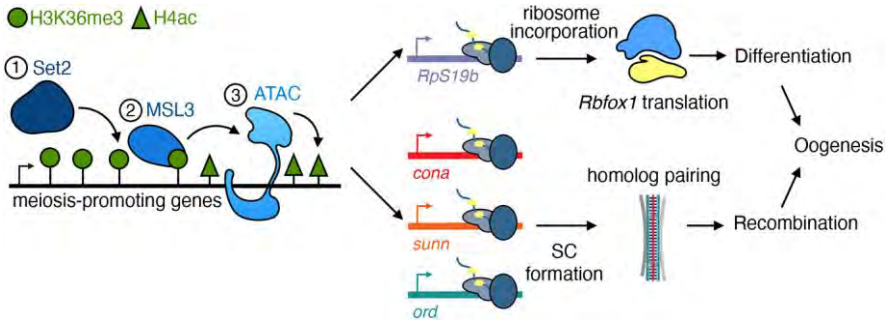

Figure 7. Schematic of how Set2, MSL3, and ATAC complex regulate oogenesis. Set2, MSL3 and ATAC complex regulates transcription of *RpS19b* and SC components. RpS19b promotes translation of differentiation factor Rbfox1 to promote oogenesis.

Supplementary Figure 1

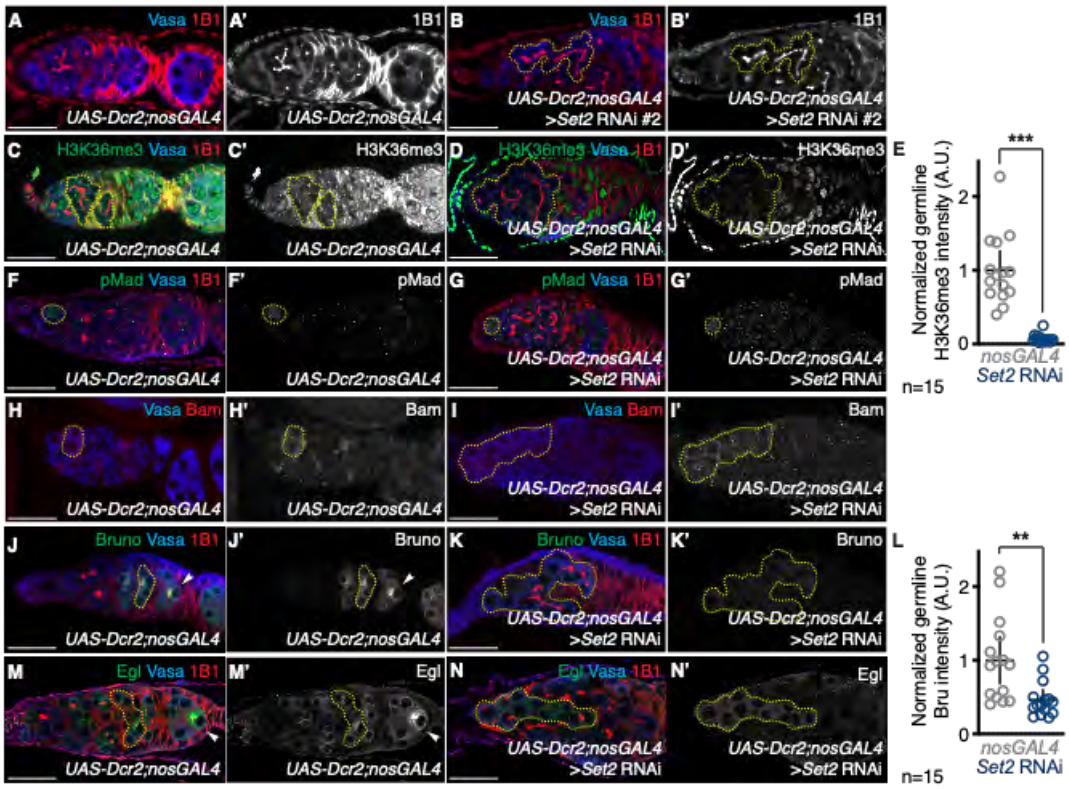

Fig. S1. Set2 is required for proper cyst formation and Rbfox1 expression.

(A-A') Control and (B-B') germline depleted *Set2* (line #2) germaria stained for Vasa (blue) and 1B1 (red) shows that *Set2* germline depletion results in irregular cysts (yellow dashed outline) (84% in *Set2* RNAi line #2 compared to 0% in *nosGAL4*; *p<2.2E-16*, n=50). Statistical analysis performed with Fisher's exact test. 1B1 channel is shown in A' and B'.

(C-C') Control and (D-D') germline depleted *Set2* germaria stained for H3K36me3 (green), Vasa (blue), and 1B1 (red) shows that *Set2* germline depletion results in decreased levels of H3K36me3 compared to control (yellow dashed outline and white arrow) (0.1±0.1 in *Set2* RNAi compared to 1.0±0.1 in *nosGAL4*; *p<0.0001*, n=15). H3K36me3 channel is shown in C' and D'. Quantitation in (E), statistical analysis performed with Student t-test; *** indicates *p<0.001*.

(F-F') Control and (G-G') germline depleted *Set2* germaria stained for pMad (green), Vasa (blue), and 1B1 (red) shows that *Set2* germline depletion does not result in an increase in number of pMad-positive germ cells compared to control (yellow dashed outline) (1.1±1.1 in *Set2* RNAi compared to 2.0±0.8 in *nosGAL4*; *p=1.9E-5*, n=50). Statistical analysis performed with Student t-test. pMad channel is shown in F' and G'.

(H-H') Control and (I-I') germline depleted *Set2* germaria stained for Vasa (blue) and Bam (red) shows that *Set2* germline depletion results in an expansion of Bam-positive germ cells compared to control (yellow dashed outline) (70% in *Set2* RNAi compared to 0% in *nosGAL4*; *p=4.1E-15*, n=50). Statistical analysis performed with Fisher's exact test. Bam channel is shown in H' and I'.

(J-J') Control and (K-K') germline depleted *Set2* germaria stained for Bruno (green), Vasa (blue), and 1B1 (red)shows that *Set2* germline depletion results in reduced levels of Bruno compared to control (yellow dashed outline and white arrow) (0.5±0.1 in *Set2* RNAi compared to 1.0±0.2 in *nosGAL4*; *p=0.0024*, n=15). Bruno channel is shown in J' and K'. Quantitation in (L), statistical analysis performed with Student t-test; ** indicates *p<0.01*.

(M-M') Control and (N-N') germline depleted *Set2* germaria stained for Egl (green), Vasa (blue), and 1B1 (red) shows that *Set2* germline depletion results in aberrant Egl localization compared to control (yellow dashed outline) (90% in *Set2* RNAi compared to 4% in *nosGAL4*; *p=9E-16*, n=50) and improper oocyte specification (white arrow). Statistical analysis performed with Fisher's exact test. Egl channel is shown in M' and N'.

Scale bar for all images is 20 μm.

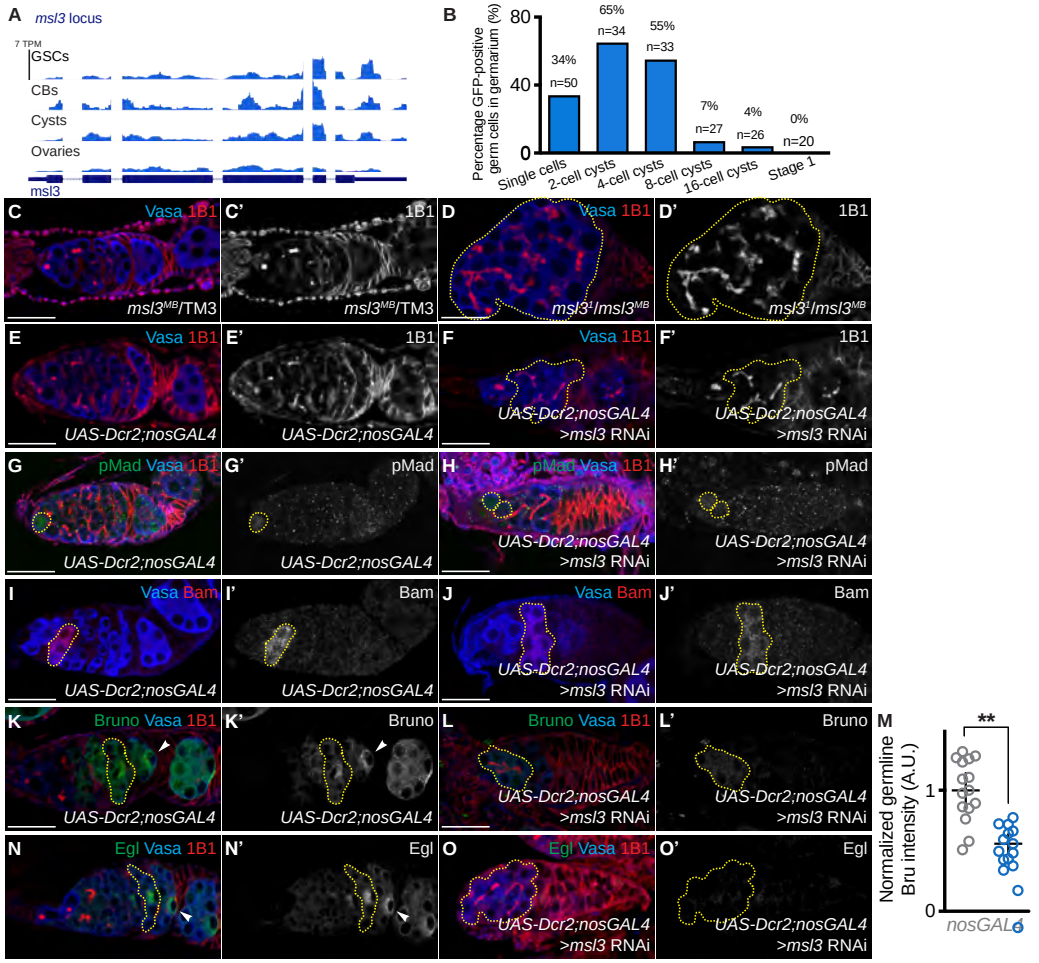

Supplementary Figure 2: MSL3 is required in the germline and works with Set2

(A) RNA-seq track showing that *msl3* is expressed during oogenesis. All tracks are set to scale to 7 TPM.

(B) Quantitation of frequency of germline MSL3-GFP expression in single cells, 2-cell cyst, 4-cell cyst, 8-cell cyst, 16-cell cyst, and stage 1 egg chambers (34% in single cells, n=50; 65% in 2-cell cyst, n=34; 55% in 4-cell cyst, n=33; 7% in 8-cell cyst, n=27; 4% in 16-cell cyst, n=26; and 0% in stage 1 egg chamber, n=20), showing that MSL3 is expressed during the mitotic and early meiotic stages of oogenesis.

(C-C') Heterozygous controls and (D-D') trans-allelic *msl3* mutant germaria stained for Vasa (blue) and 1B1 (red) shows that *msl3* mutants have irregular cysts (yellow dashed outline) (62% in $msl3^{1}/msl3^{MB}$ compared to 0% in $msl3^{1}$ and $msl3^{MB}$ heterozygotes; *p=1.7E-07*, n=72) and germline loss (38% in $msl3^{1}/msl3^{MB}$ compared to 0% in $msl3^{1}$ and $msl3^{MB}$ heterozygotes; *p<2.2E-16*, n=72). 1B1 channel is shown in C', and D'. Quantitation in Figure 2D.

(E-E') Control and (F-F') germline depleted *msl3* germaria stained for Vasa (blue) and 1B1 (red) shows that *msl3* germline depletion results in irregular cyst formation (yellow dashed outline) (87% in *msl3* RNAi compared to 0% in *nosGAL4*; *p<2.2E-16*, n=70) and germline loss (13% in *msl3* RNAi compared to 0% in *nosGAL4*; *p<2.2E-16*, n=70). 1B1 channel is shown in E' and F'. Quantitation in Figure 2D.

(G-G') Control and (H-H') germline depleted *msl3* germaria stained for pMad (green), Vasa (blue), and 1B1 (red) shows that *msl3* germline depletion does not result in an increase in number of pMad-positive germ cells compared to control (yellow dashed outline) (1.0±0.9 in *msl3* RNAi compared to 2.0±0.7 in *nosGAL4*; *p=1.1E-5*, n=30). Statistical analysis performed with Student t-test. pMad channel is shown in G' and H'.

(I-I') Control and (J-J') germline depleted *msl3* germaria stained for Vasa (blue) and Bam (red) shows that *msl3* germline depletion results in an expansion of Bam-positive germ cells compared to control (yellow dashed outline) (26% in *msl3* RNAi compared to 0% in *nosGAL4*; *p<3.5E-10*, n=50). Statistical analysis performed with Fisher's exact test. Bam channel is shown in I' and J'.

(K-K') Control and (L-L') germline depleted *msl3* germaria stained for Bruno (green), Vasa (blue), and 1B1 (red) shows that *msl3* germline depletion results in reduced levels of Bruno compared to control (yellow dashed outline and white arrow) (0.56±0.04 in *msl3* RNAi compared to 1.0±0.07 in *nosGAL4*; *p<0.0001*, n=15). Bruno channel is shown in K' and L'. Quantitation in (M), statistical analysis performed with Student t-test; *** indicates *p<0.001*.

(N-N') Control and (O-O') germline depleted *msl3* germaria stained for Egl (green), Vasa (blue), and 1B1 (red) shows that *msl3* germline depletion results in aberrant Egl localization compared to control (yellow dashed outline) (96% in *msl3* RNAi compared to 0% in *nosGAL4*; *p<2.2E-16*, n=50) and improper oocyte specification (white arrow). Statistical analysis performed with Fisher's exact test. Egl channel is shown in N' and O'.

Scale bar for all images is 20 μm.

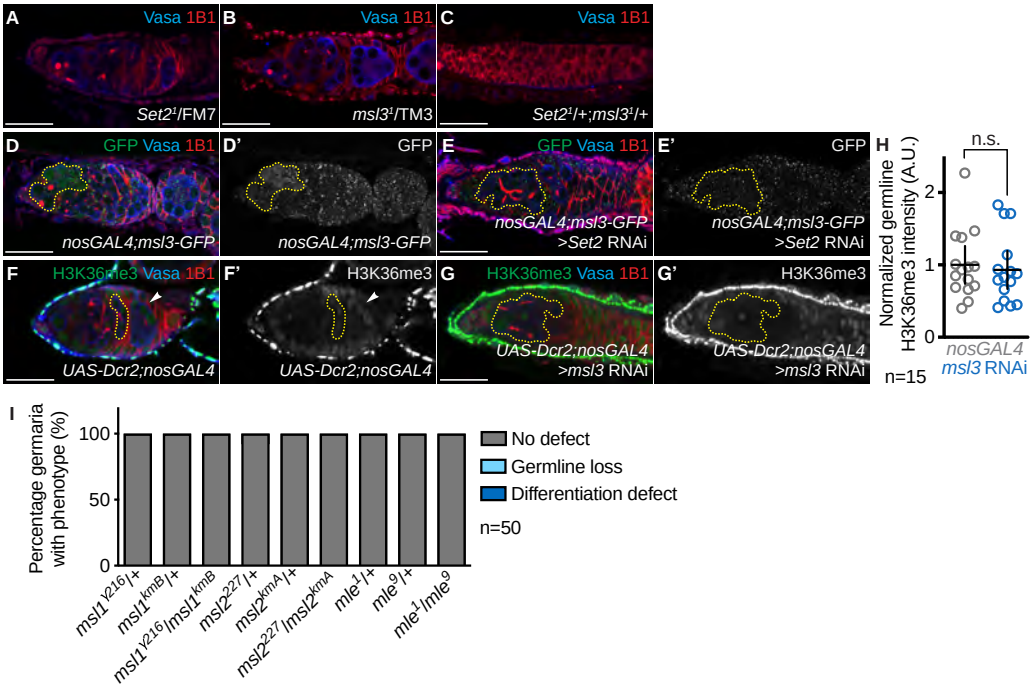

Fig. S3. MSL3 works independently of MSL complex in the ovaries

(A-B) Heterozygous controls and (C) trans-heterozygous *Set2¹/+;msl3¹/+* mutant germaria stained for Vasa (blue) and 1B1 (red) shows that trans-heterozygotes have severe germline loss compared to heterozygous control (100% in *Set2¹/+;msl3¹/+* compared to 0% in *Set2¹* heterozygotes and 0% in *msl3¹* heterozygotes; *p<2.2E-16* for both, n=50). Statistical analysis performed with Fisher's exact test.

(D-D') Control and (E-E') germline depleted *Set2* germaria stained for GFP (green), Vasa (blue), and 1B1 (red) shows that *Set2* germline depletion results in aberrant MSL3-GFP localization compared to control (yellow dashed outline) (100% in *Set2* RNAi compared to 3.3% in *nosGAL4;msl3-GFP*; *p=5.2E-16*, n=30). Statistical analysis performed with Fisher's exact test. GFP channel is shown in D' and E'.

(F-F') Control and (G-G') germline depleted *msl3* germaria stained for H3K36me3 (green), Vasa (blue), and 1B1 (red) shows that *msl3* germline depletion results in unchanged levels of H3K36me3 compared to control (yellow dashed outline and white arrow) (0.9±0.1 in *msl3* RNAi compared to 1.0±0.1 in *nosGAL4*; *p=0.69*, n=15). H3K36me3 channel is shown in F' and G'. Quantitation in (H), statistical analysis performed with Student t-test; "n.s." *p>0.5*.

(I) Percentage heterozygous controls and trans-allelic MSL complex mutants with no defect (gray), germline loss (light blue), and differentiation defect (dark blue). *msl1*, *msl2*,

and *mle* mutants do not show irregular cyst formation or germline loss compared to respective heterozygous controls (100% in $msl1^{\gamma 216}$/+;$msl1^{kmB}$/+ compared to 100% in $msl1^{\gamma 216}$ and $msl1^{kmB}$ heterozygotes; *p=1*, n=50; 100% in $msl2^{227}$/+;$msl2^{kmA}$/+ compared to 100% and 100% in $msl2^{227}$ and $msl2^{kmA}$ heterozygotes; *p=1* for both, n=50; 100% in mle^{1}/+;mle^{9}/+ compared to 100% in mle^{1} and mle^{9} heterozygotes; *p=1* for both, n=50). Statistical analysis performed with Fisher's exact test on differentiation defect. No statistical significance was found.

Scale bar for all images is 20 μm.

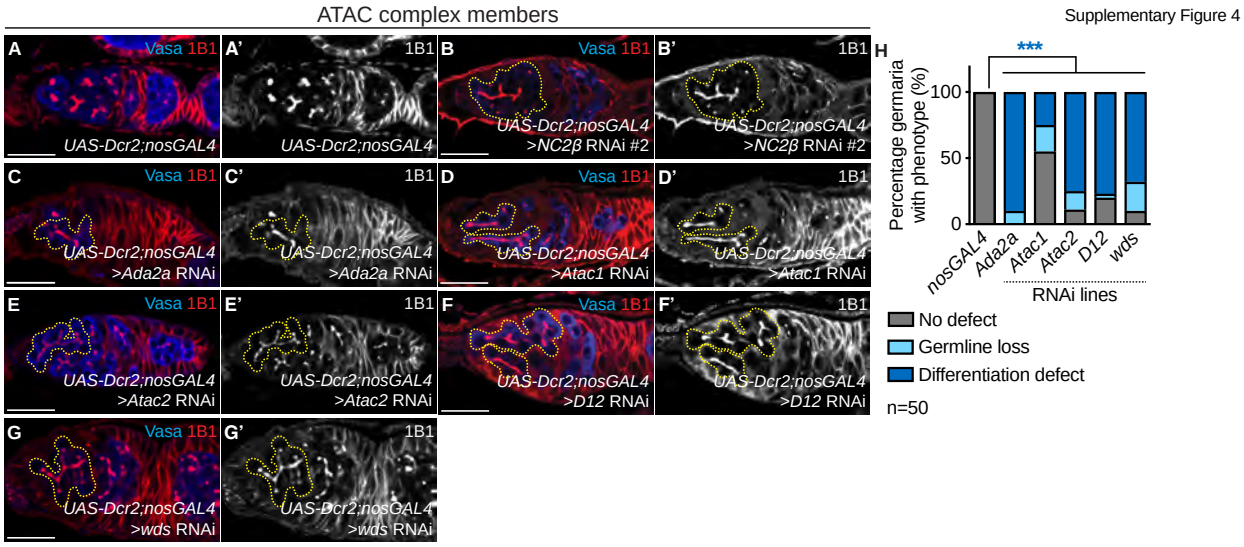

Fig. S4. ATAC members are required in the germline for proper cyst formation

(A-A') Control, germline depleted (B-B') *NC2β*, (C-C') *Ada2a*, (D-D') *Atac1*, (E-E') *Atac2*, (F-F') *D12*, and (G-G') *wds* germaria stained for Vasa (blue) and 1B1 (red) shows that ATAC member germline depletion results in irregular cysts (yellow dashed outline) (24% in *NC2β* RNAi line #2, 90% in *Ada2a* RNAi, 24% in *Atac1* RNAi, 76% in *Atac2* RNAi, 78% in *D12* RNAi, and 68% in *wds* RNAi compared to 0% *nosGAL4*; $p<0.0001$ for all, n=50) and germline loss (22% in *NC2β* RNAi line #2, 10% in *Ada2a* RNAi, 20% in *Atac1* RNAi, 14% in *Atac2* RNAi, 4% in *D12* RNAi, and 22% in *wds* RNAi compared to 0% in *nosGAL4*; $p<0.05$ for *Atac1*, *Atac2*, and *wds* RNAi, $p>0.05$ for *Ada2a* and *D12* RNAi, n=50). 1B1 channel is shown in A', B', C', D', E', F', and G'. Quantitation in (H), statistical analysis performed with Fisher's exact test on differentiation defect; *** indicates $p<0.001$.

Scale bar for all images is 20 μm.

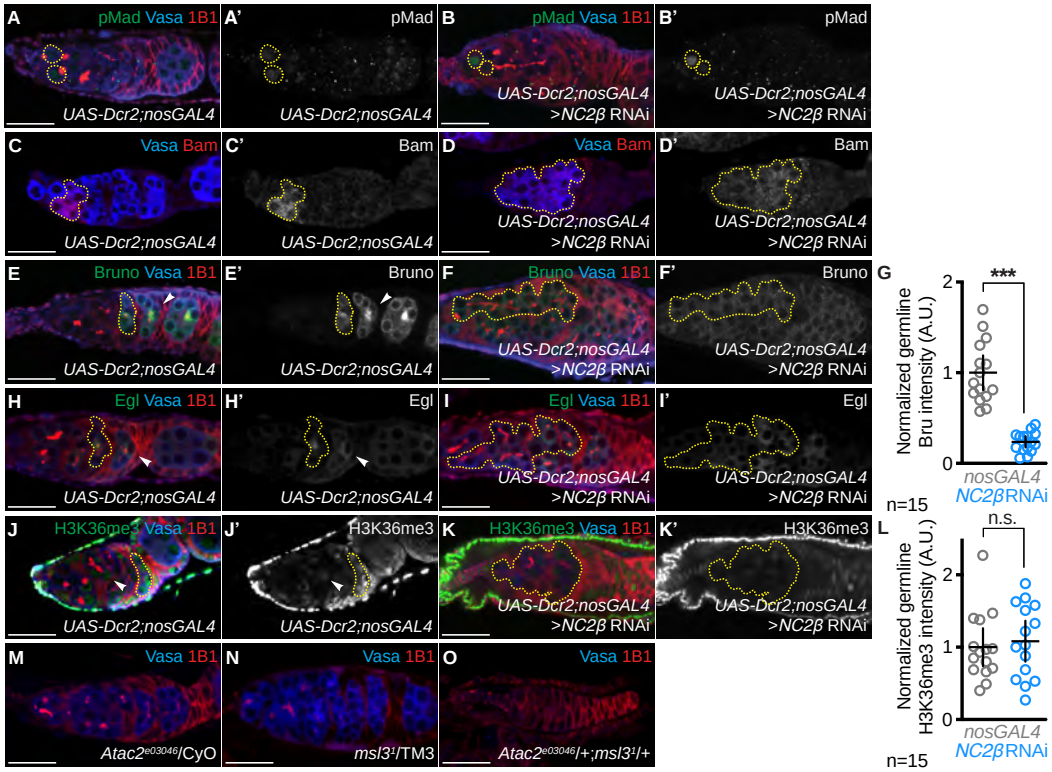

Fig. S5. NC2β, an ATAC complex component, is required in the germline for proper differentiation and oocyte specification

(A-A') Control and (B-B') germline depleted *NC2β* germaria stained for pMad (green), Vasa (blue), and 1B1 (red) shows that *NC2β* germline depletion does not result in an increase in number of pMad-positive germ cells compared to control (yellow dashed outline) (1.4±1.3 in *NC2β* RNAi compared to 2.1±0.7 in *nosGAL4*; *p<0.0001*, n=50). Statistical analysis performed with Student t-test. pMad channel is shown in A' and B'.

(C-C') Control and (D-D') germline depleted *NC2β* germaria stained for Vasa (blue) and Bam (red) shows that *NC2β* germline depletion results in an expansion of Bam-positive germ cells compared to control (yellow dashed outline) (70% in *NC2β* RNAi compared to 0% in *nosGAL4*; *p=4.1E-15*, n=50). Statistical analysis performed with Fisher's exact test. Bam channel is shown in C' and D'.

(E-E') Control and (F-F') germline depleted *NC2β* germaria stained for Bruno (green), Vasa (blue), and 1B1 (red) shows that *NC2β* germline depletion results in reduced levels of Bruno compared to control (yellow dashed outline and white arrow) (0.2±0.1 in *NC2β* RNAi compared to 1.0±0.3 in *nosGAL4*; *p<0.0001*, n=15). Bruno channel is shown in E' and F'. Quantitation in (G), statistical analysis performed with Student t-test; *** indicates *p<0.001*.

(H-H') Control and (I-I') germline depleted *NC2β* germaria stained for Egl (green), Vasa (blue), and 1B1 (red) shows that *NC2β* germline depletion results in aberrant Egl localization compared to control (yellow dashed outline) (72% in *NC2β* RNAi compared to 0% in *nosGAL4* germaria; *p=9.5E-16*, n=50) and improper oocyte specification (white arrow). Statistical analysis performed with Fisher's exact test. Egl channel is shown in H' and I'.

(J-J') Control and (K-K') germline depleted *NC2β* germaria stained for H3K36me3 (green), Vasa (blue), and 1B1 (red) shows that *NC2β* germline depletion results in unchanged levels of H3K36me3 compared to control (yellow dashed outline) (1.1±0.5 in *NC2β* RNAi compared to 1.0±0.5 in *nosGAL4*; *p=0.65*, n=15). H3K36me3 channel is shown in J' and K'. Quantitation in (L), statistical analysis performed with Student t-test; "n.s." indicates *p>0.5*.

(M-N) Heterozygous controls and (O) trans-heterozygous $Atac2^{e03046}$/+;$msl3^{1}$/+ mutant germaria stained for Vasa (blue) and 1B1 (red) shows that trans-heterozygotes have severe germline loss compared to heterozygous controls (100% in $Atac2^{e03046}$/+;$msl3^{1}$/+ compared to 0% in $msl3^{1}$ and $Atac2^{e03046}$ heterozygotes; *p=1.6E-14* for both, n=25). Statistical analysis performed with Fisher's exact test on differentiation defect.

Scale bar for all images is 20 μm.

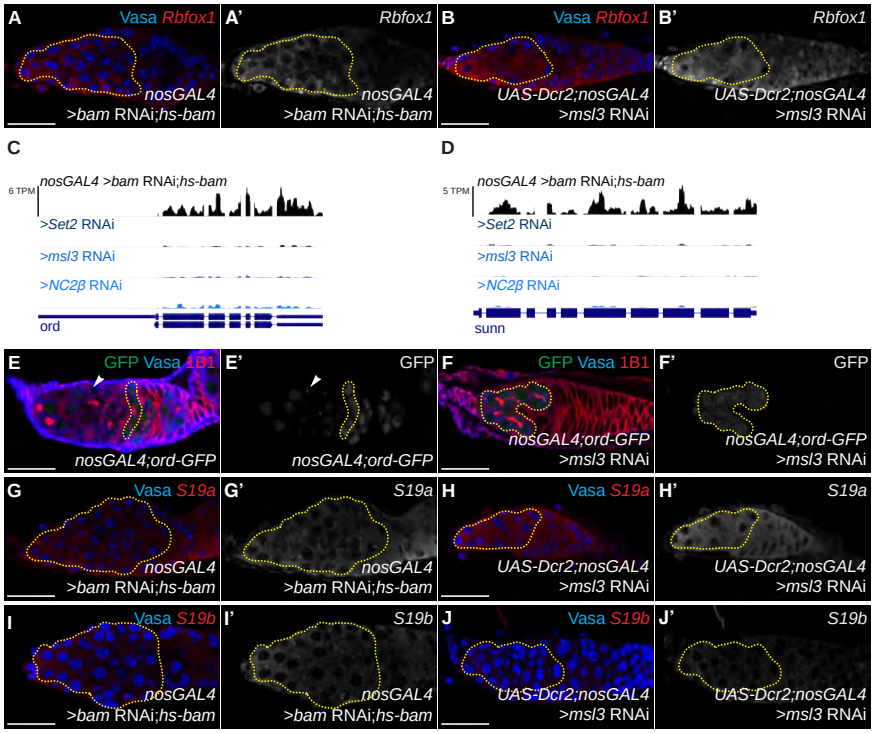

Fig. S6. MSL3 regulates levels of meiosis- promoting genes and the germline-enriched ribosomal protein, *RpS19b*

(A-A') Control and (B-B') germline depleted *msl3* germaria stained for RNA probes against *Rbfox1* (red) and DAPI (blue) shows that *msl3* germline depletion results in unchanged *Rbfox1* levels in the germline compared to control (1.0±0.3 in *msl3* RNAi compared to 1.0±0.2 in *bam* RNAi;*hs-bam*; *p=0.66*, n=15). Statistical analysis performed with Student t-test. *Rbfox1* channel is shown in A' and B'.

(C) RNA-seq track showing that *ord* is reduced upon germline depletion of *Set2*, *msl3*, and *NC2β*. All tracks are set to scale to 5 TPM.

(D) RNA-seq track showing that *sunn* is reduced upon germline depletion of *Set2*, *msl3*, and *NC2β*. All tracks are set to scale to 6 TPM.

(E-E') Control and (F-F') germline depleted *msl3* germaria stained for GFP (green), Vasa (blue), and 1B1 (red) shows that *msl3* germline depletion results in lower and mislocalized GFP levels compared to control (0.5±0.2 in *msl3* RNAi compared to 1.0±0.2 in *bam* RNAi;*hs-bam*; *p<0.0001*, n=15). Statistical analysis performed with Student t-test. GFP channel is shown in E' and F'.

(G-G') Control and (H-H') germline depleted *msl3* germaria stained for RNA probes against *RpS19a* (red) and DAPI (blue) shows that *msl3* germline depletion results in unchanged *RpS19a* levels in the germline compared to control (1.0±0.4 in *msl3* RNAi compared to 0.9±0.4 in *bam* RNAi;*hs-bam*; *p=0.35*, n=15). Statistical analysis performed with Student t-test. *RpS19a* channel is shown in G' and H'.

(I-I') Control and (J-J') germline depleted *msl3* germaria stained for RNA probes against *RpS19b* (red) and DAPI (blue) shows that *msl3* germline depletion results in lower *RpS19b* levels in the germline compared to control (0.4±0.2 in *msl3* RNAi compared to 1.0±0.3 in *bam* RNAi;*hs-bam*; *p<0.0001*, n=15). Statistical analysis performed with Student t-test. *RpS19b* channel is shown in I' and J'.

Scale bar for all images is 20 μm.

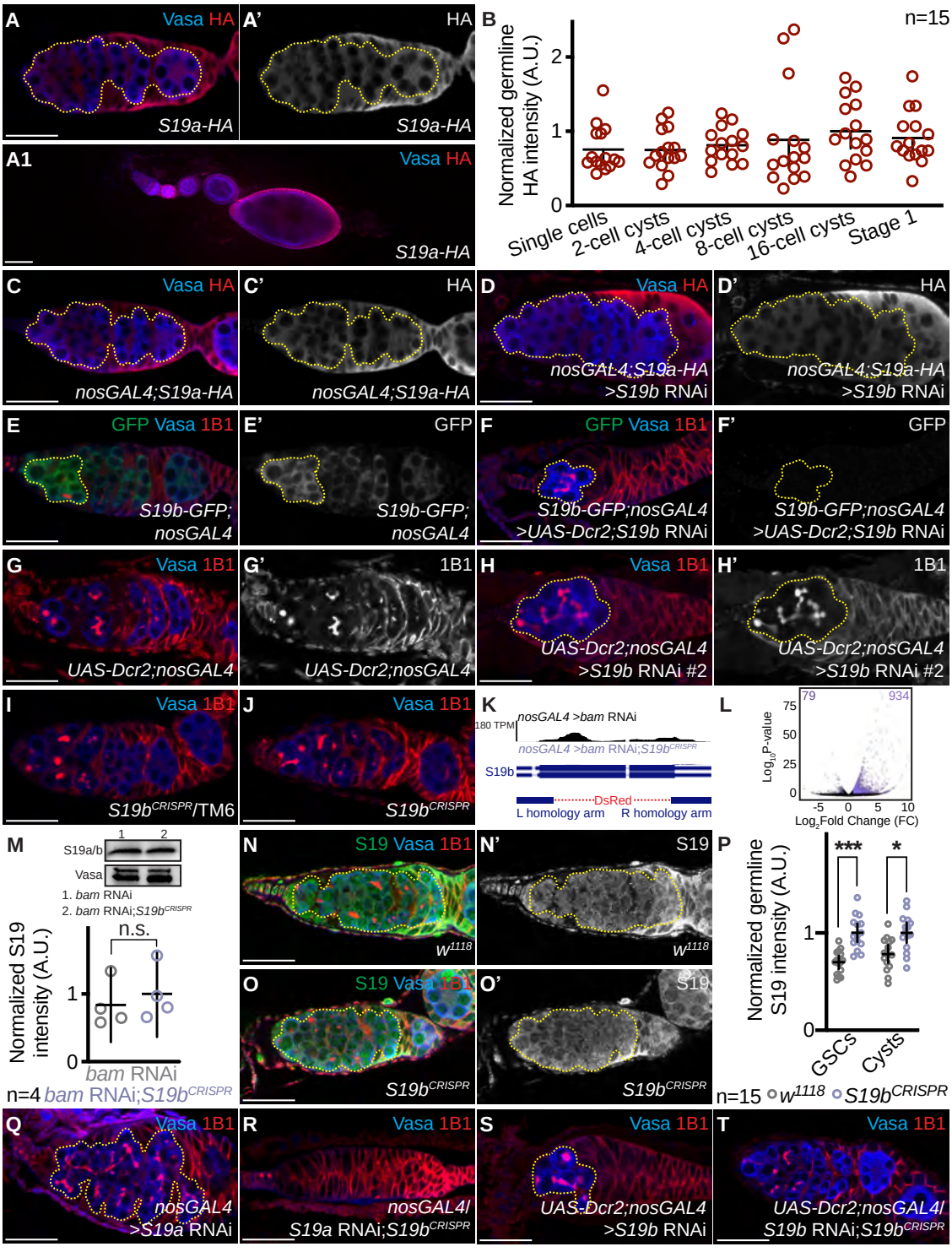

Fig. S7. RpS19a is in the germline and soma of *Drosophila* ovaries

(A-A') *RpS19a-HA* germarium and (A1) ovariole stained for Vasa (blue) and HA (red) shows that HA expression is in soma and germline (0.8±0.1 in single cells, 0.8±0.1 in 2-cell cyst, 0.8±0.1 in 4-cell cyst, 0.9±0.2 in 8-cell cyst, 1.0±0.1 in 16-cell cyst, and 0.9±0.1

in stage 1 egg chamber; *p>0.5*, n=15). HA channel is shown in A'. Quantitation in (B), statistical analysis performed with one-way ANOVA; "n.s." indicates *p>0.5.*

(C-C') Control and (D-D') germline depleted *RpS19b* germaria stained for Vasa (blue) and HA (red) shows that *RpS19b* germline depletion does not result in decreased RpS19a-HA compared to control (1.3±0.2 in *RpS19b* RNAi compared to 1.0±0.2 in *nosGAL4*; *p>0.05*, n=15). Statistical analysis performed with Student t-test. HA channel is shown in C', and D'.

(E-E') Control and (F-F') germline depleted *RpS19b* germaria stained for GFP (green), Vasa (blue) and 1B1 (red) shows that *RpS19b* germline depletion results in decreased RpS19b-GFP expression compared to control (0.6±0.3 in *RpS19b* RNAi compared to 1.0±0.2 in *nosGAL4*; *p=0.013*, respectively, n=15). Statistical analysis performed with Student t-test. GFP channel is shown in E' and F'.

(G-G') Control and (H-H') germline depleted *RpS19b* (line #2) germaria stained for Vasa (blue) and 1B1 (red) shows that *RpS19b* germline depletion results in accumulation of irregular cysts (yellow dashed outline) (32% in *RpS19b* RNAi line #2 compared to 0% in *nosGAL4*; *p=7.3E-6*, n=50). Statistical analysis performed with Fisher's exact test. 1B1 channel is shown in G' and H'.

(I) Heterozygous and (J) homozygous $RpS19b^{CRISPR}$ mutant germaria stained for Vasa (blue) and 1B1 (red) shows that *RpS19b* mutants do not show cyst defects compared to heterozygous control (97% in *RpS19b* homozygotes compared to 100% in *RpS19b* heterozygotes; *p=1*, n=30). Statistical analysis performed with Fisher's exact test.

(K) Top: RNA-seq track showing that *RpS19b* reads are reduced in *bam* RNAi;$RpS19b^{CRISPR}$ compared to *bam* RNAi. All tracks are set to scale to 120 TPM. Below: Schematic of $RpS19b^{CRISPR}$ mutant design.

(L) Biplot of Log_2(TPM)*bam* RNAi;$S19b^{CRISPR}$ vs. Log_2(TPM)*bam* RNAi of *bam* RNAi. Light purple dots represent significantly downregulated transcripts and dark purple dots represent significantly upregulated transcripts in *bam* RNAi;$S19b^{CRISPR}$ ovaries compared with *bam* RNAi ovaries. Genes with four-fold or higher change were considered significant.

(M) Top: Western blot analysis of *bam* RNAi and *bam* RNAi;$S19b^{CRISPR}$ ovaries. The blot was stained for RpS19 and Vasa showing that RpS19 levels are not significantly decreased in *bam* RNAi;$RpS19b^{CRISPR}$ compared to *bam* RNAi (1.0±0.2 in $RpS19b^{CRISPR}$

compared to 0.8±0.2 in *bam* RNAi; *p=0.5594*, n=4. Bottom: Quantitation, statistical analysis performed with Student t-test; "n.s." indicates *p>0.5*.

(N-N') Control and (O-O') *RpS19b*^{CRISPR} germaria stained for RpS19 (green), Vasa (blue), and 1B1 (red) shows that *RpS19b*^{CRISPR} germaria do not have decreased RpS19 expression compared to control (1.0±0.2 in *RpS19b*^{CRISPR} GSCs compared to 0.7±0.1 in *w*^{1118} GSCs; *p<0.0001*, n=15; 1.0±0.2 in *RpS19b*^{CRISPR} cysts compared to 0.8±0.2 in *w*^{1118} cysts; *p=0.0023*, n=15). S19 channel is shown in N' and O'. Quantitation in (P), statistical analysis performed with Student t-test; * indicates *p.0.05* and ** indicates *p<0.001*.

(Q) Germline depleted *RpS19a* and (R) germline depleted of *RpS19a* in homozygous *RpS19b*^{CRISPR} mutant germaria stained for Vasa (blue) and 1B1 (red) shows that *RpS19a* germline depletion in *RpS19b*^{CRISPR} mutants results in germline loss compared to germaria with germline depletion of *RpS19a* (yellow dashed outline) (78% in *RpS19a* RNAi;*RpS19b*^{CRISPR} compared to 20% in *RpS19a* RNAi; *p<2.2E-16*, n=50). Statistical analysis performed with Fisher's exact test.

(S) Germline depleted *RpS19b* and (T) germline depleted of *RpS19b* in homozygous *RpS19b*^{CRISPR} mutant germaria stained for Vasa (blue) and 1B1 (red) shows that *RpS19b* germline depletion in *RpS19b*^{CRISPR} mutants results in no defects compared to germaria with germline depletion of *RpS19b* (yellow dashed outline) (100% in *RpS19b* RNAi;*RpS19b*^{CRISPR} compared to 26% in *RpS19b* RNAi; *p<2.2E-16*, n=50). Statistical analysis performed with Fisher's exact test.

Scale bar for all images is 20 μm.

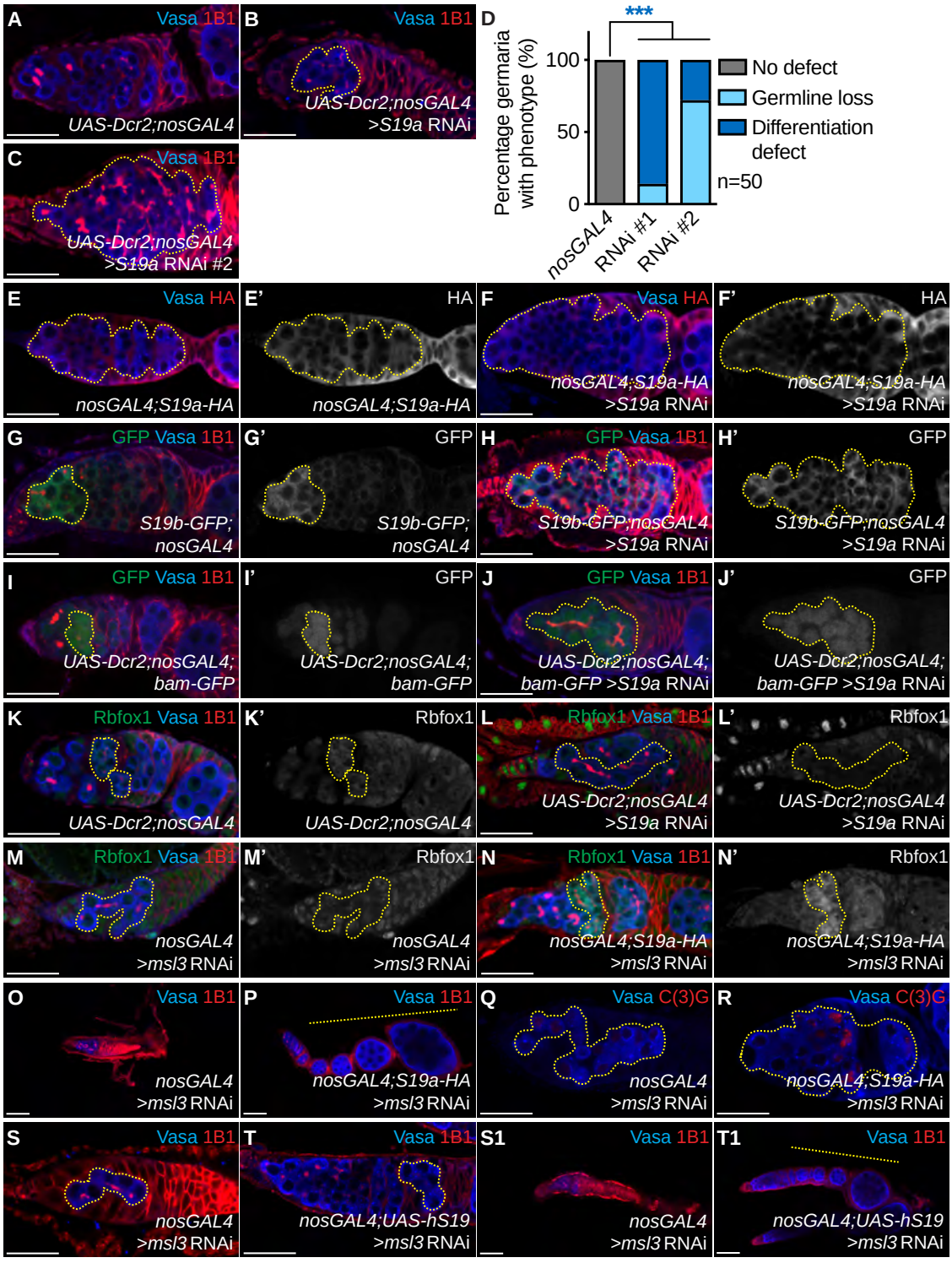

Fig. S8. RpS19a rescues *msl3* differentiation defect but not meiotic progression defect

(A) Control and (B-C) germline depleted *RpS19a* (RNAi line #1 and 2) germaria stained for Vasa (blue) and 1B1 (red) shows that *RpS19a* germline depletion results in irregular cysts (yellow dashed outline) (90% in *RpS19a* RNAi line #1 and 60% in *RpS19a* RNAi line #2 compared to 0% in *nosGAL4*; $p<2.2E-16$ and $p=3.1E-15$, respectively, n=50) and germline loss (10% in *RpS19a* RNAi line #1 and 40% in *RpS19a* RNAi line #2 compared to 0% in *nosGAL4*; $p>0.05$ and $p=5.5E-9$, respectively, n=50). Quantitation in (D), statistical analysis performed with Fisher's exact test on differentiation defect; *** indicates $p<0.001$.

(E-E') Control and (F-F') germline depleted *RpS19a* germaria stained for Vasa (blue) and HA (red) shows that *RpS19a* germline depletion results in decreased RpS19a-HA expression compared to control (0.3±0.2 in *RpS19a* RNAi compared to 1.0±0.7 in *nosGAL4*; $p=0.005$ n=15). Statistical analysis performed with Student t-test. HA channel is shown in E' and F'.

(G-G') Control and (H-H') germline depleted *RpS19a* germaria stained for GFP (green), Vasa (blue) and 1B1 (red) shows that *RpS19a* germline depletion does not result in decreased RpS19b-GFP expression compared to control (1.7±0.5 in *RpS19a* RNAi compared to 1.0±0.3 in *nosGAL4*; $p<0.0001$, n=15). Statistical analysis performed with Student t-test. GFP channel is shown in G' and H'.

(I-I') Control and (J-J') germline depleted *RpS19a* germaria both carrying a *bam-GFP* transgene stained for GFP (green), Vasa (blue), and 1B1 (red) shows that *RpS19a* germline depletion results in irregular GFP-positive cysts compared to control (yellow dashed outline) (80% in *RpS19a* RNAi compared to 0% in *nosGAL4*; $p=2.5E-13$, n=50). Statistical analysis performed with Fisher's exact test. GFP channel is shown in I' and J'.

(K-K') Control and (L-L') germline depleted *RpS19a* germaria stained for Rbfox1 (green), Vasa (blue), and 1B1 (red) shows that *RpS19a* germline depletion results in decreased levels of Rbfox1 in the germline compared to control (yellow dashed outline) (0.6±0.4 in *RpS19a* RNAi compared to 1.0±0.6 in *nosGAL4*; $p=0.04$, n=15). Statistical analysis performed with Student t-test. Rbfox1 channel is shown in K' and L'.

(M-M') Control and (N-N') *RpS19a-HA* rescue germaria stained for Rbfox1 (green), Vasa (blue), and 1B1 (red) shows that addition of *RpS19a-HA* to *msl3* depletion ovaries results in increased Rbfox1 levels compared to control (1.0±0.8 in rescue compared to 0.2±0.04 in *msl3* RNAi; $p=0.0012$, n=15). Statistical analysis performed with Student t-test. Rbfox1 channel is shown in M' and N'.

(O) Control and (P) *RpS19a-HA* rescue germaria stained for Vasa (blue) and 1B1 (red) shows that addition of *RpS19a-HA* to *msl3* depletion ovaries results in an increased frequency of spectrosomes and cysts (86% in *RpS19a-HA* rescue compared to 18% in *msl3* RNAi; *p=1.5E-8*, n=50) and subsequent egg chambers compared to control (yellow dashed outline) (78% in *RpS19a-HA* rescue compared to 18% in *msl3* RNAi; *p=2.1E-9*, n=50). Statistical analysis performed with Fisher's exact test.

(Q) Control and (R) *RpS19a-HA* rescue germaria stained for Vasa (blue) and C(3)G (red) shows that rescue and control germaria both have aberrant C(3)G expression (yellow dashed outline and white arrows) (85% in *RpS19a-HA* rescue compared to 100% in *msl3* RNAi; *p=0.23*, n=50). Addition of *RpS19a-HA* does not rescue egg laying defects (28 eggs/female in *RpS19a-HA* compared to 0 eggs/female in *msl3* RNAi and rescue; *p<0.0004*, n=4). Statistical analysis performed with Fisher's exact test.

(S) Control and (T) *hRpS19-HA* rescue germaria stained for Vasa (blue) and 1B1 (red) shows that expression of *UAS-hRpS19-HA* in *msl3* germline depletion ovaries results in single cells and cysts compared to control (yellow dashed outline) (96% in *hRpS19-HA* rescue compared to 22% in *msl3* RNAi; *p=7.6E-9*, n=40). Statistical analysis performed with Fisher's exact test.

(S1) Control and (T1) *hRpS19-HA* rescue ovarioles stained for Vasa (blue) and 1B1 (red) shows that expression of *UAS-hRpS19-HA* in *msl3* germline depletion ovaries results in an increased frequency of subsequent egg chambers compared to control (yellow dashed outline) (100% in *hRpS19-HA* rescue compared to 15% in *msl3* RNAi; *p<2.2E-16*, n=40). Statistical analysis performed with Fisher's exact test.

Scale bar for all images is 20 μm.

Table S1. List of chromodomain containing genes screened in the germline, BDSC stock number, and a description of the resulting phenotype.

Click here to download Table S1

Table S2. Log fold change values and FDR of Tab 1: SET2 and Msl3 regulated targets; Tab 2: Msl3 and NC2b regulated targets; Tab 3: SET2 and NC2b regulated targets and Tab4: SET2, MSL3 and NC2b regulated targets

Click here to download Table S2